

# PLSO: A generative framework for decomposing nonstationary timeseries into piecewise stationary oscillatory components

Andrew H. Song<sup>1</sup>, Demba Ba<sup>2</sup>, and Emery N. Brown<sup>3,4,5,6</sup>

<sup>1</sup>Electrical Engineering and Computer Science, Massachusetts Institute of Technology, Cambridge, MA

<sup>2</sup>School of Engineering and Applied Sciences, Harvard University, Cambridge, MA

<sup>3</sup>Department of Brain and Cognitive Sciences, Massachusetts Institute of Technology, Cambridge, MA

<sup>4</sup>Institute of Medical Engineering and Sciences, Massachusetts Institute of Technology, Cambridge, MA

<sup>5</sup>Department of Anesthesia, Critical Care, and Pain Medicine, Massachusetts General Hospital, Boston, MA

<sup>6</sup>Picower Institute of Learning and Memory, Massachusetts Institute of Technology, Cambridge, MA

## Abstract

To capture the slowly time-varying spectral content of real-world time series, a common paradigm is to partition the data into approximately stationary intervals and perform inference in the time-frequency domain. This approach, however, lacks a corresponding nonstationary time-domain generative model for the entire data and thus, time-domain inference, such as sampling from the posterior, occurs in each interval separately. This results in distortion/discontinuity around interval boundaries and, consequently, can lead to erroneous inferences based on any quantities derived from the posterior, such as the phase. To address these shortcomings, we propose the Piecewise Locally Stationary Oscillation (PLSO) generative model for decomposing time-series data with slowly time-varying spectra into several oscillatory, piecewise-stationary processes. PLSO, being a nonstationary time-domain generative model, enables inference on the entire time-series, without boundary effects, and, at the same time, provides a characterization of its time-varying spectral properties. We propose a novel two-stage inference algorithm that combines the classical Kalman filter and the recently-proposed accelerated proximal gradient algorithm to optimize the nonconvex Whittle likelihood from PLSO. We demonstrate these points through experiments on simulated data and real neural data from the rat and the human brain.

## 1 Introduction

With the collection of long time-series now common, in areas such as neuroscience and geophysics, it is important to develop an *inference* framework for data where the stationarity assumption is too restrictive. We restrict our attention to data 1) with spectral properties that change slowly over time and 2) for which decomposition into several oscillatory components is warranted for interpretation, often the case in electroencephalogram (EEG) or electrophysiology recording. One can use bandpass filtering [Oppenheim et al., 2009] or methods such as the empirical mode decomposition [Huang et al., 1998, Daubechies et al., 2011] for these purposes. However, due to the absence of a generative model, these methods lack a framework for performing inference. Another approach is to perform inference in the time-frequency (TF) domain on the short-time Fourier transform (STFT) of the data, assuming stationarity within small intervals. This has led to a rich literature on inference in the TF domain [Wilson et al., 2008, Le Roux et al., 2010]. A drawback is that most of these methods focus on estimates for the power spectral density (PSD) and lose important phase information. To recover the time-domain estimates, additional algorithms are required [Griffin and Jae Lim, 1984].

This motivates us to explore time-domain generative models, which allow for time-domain inference and decomposition into oscillatory components. We can find such examples in the signal processing/Gaussian process (GP) communities, assuming stationarity. A superposition of stochastic harmonic oscillators, where each oscillator corresponds to a frequency band, is used in the processing of speech [Cemgil and Godsill, 2005] and neuroscience data [Matsuda and Komaki, 2017, Beck et al., 2018]. In GP [Rasmussen and Williams, 2005], the spectral mixture (SM) kernel [Wilson and Adams, 2013, Wilkinson et al., 2019] model the data as samples from a GP, whose kernel consists of the superposition of localized and frequency-modulated kernels.

These time-domain models can be applied to nonstationary data by partitioning them into stationary intervals. Compared to STFT-based methods, time-domain models retain phase information. This allows time-domain inference within each interval. Nevertheless, we are faced with a different kind of challenge. As the inference is localized within each interval, the time-domain estimates in different intervals are independent conditioned on the time-series data and, therefore, do not reflect the dependence across intervals. This also causes discontinuity/distortion of the time-domain estimates near the interval boundaries, and consequently any quantities derived from these estimates.

To address these shortcomings, we propose a generative framework for data with slow time-varying spectra, termed the Piecewise Locally Stationary Oscillation (PLSO) framework. The main contributions are:

**Generative model for piecewise stationary, oscillatory components** PLSO is a time-domain generative

framework that models time-series as the superposition of piecewise stationary, oscillatory components. This allows time-domain inference on each component and estimation of the time-varying spectra.

**Continuity across stationary intervals** The state-space model that underlies PLSO strikes a balance between ensuring time-domain continuity across piecewise stationary intervals and stationarity within each interval. Moreover, by imposing stochastic continuity on the interval-level, PLSO learns underlying smooth time-varying spectra accurately.

**Inference procedure** We propose a two-stage inference procedure for the time-varying spectra and the corresponding time-series. By leveraging the Markovian dynamics of our model, the algorithm combines Kalman filter theory [Kalman, 1960] and inexact accelerated proximal gradient approach [Li and Lin, 2015].

In Section 2 we introduce necessary background, followed by the PLSO framework in Section 3. In Section 4, we discuss inference for PLSO. In Section 5, we present experimental results and conclude in Section 6.

## 2 Background

### 2.1 Notation

We use  $j \in \{1, \dots, J\}$  and  $k \in \{1, \dots, K\}$  to denote frequency index and discrete-time sample index, respectively. We use  $\omega \in [-\pi, \pi]$  for normalized frequency. The  $j^{\text{th}}$  latent stochastic process is denoted as  $\mathbf{z}_j \in \mathbb{C}^K$ , with  $\mathbf{z}_{j,k} \in \mathbb{C}$  denoting the  $k^{\text{th}}$  sample of  $\mathbf{z}_j$  and  $\mathbf{z}_{j,k}^{\Re}, \mathbf{z}_{j,k}^{\Im}$  its real and imaginary parts. To denote the elements of  $\mathbf{z}_j$ , we use  $\mathbf{z}_{j,k:k'} = (\mathbf{z}_{j,k}, \dots, \mathbf{z}_{j,k'})^{\text{T}}$ . We also represent  $\mathbf{z}_{j,k}$  as a  $\mathbb{R}^2$  vector,  $\mathbf{z}_{j,k}^{\text{vec}} = [\mathbf{z}_{j,k}^{\Re}, \mathbf{z}_{j,k}^{\Im}]^{\text{T}}$ . The state covariance matrix for  $\mathbf{z}_{j,k}$  is defined as  $\mathbf{P}_j^k = \mathbb{E} \left[ \mathbf{z}_{j,k}^{\text{vec}} \left( \mathbf{z}_{j,k}^{\text{vec}} \right)^{\text{T}} \right]$ . We use  $m \in \{1, \dots, M\}$  to denote each interval of length  $N$  and  $n \in \{1, \dots, N\}$  to indicate the sample index *within* each window.

### 2.2 Continuous-time/discrete-time model

Let  $y(t)$  be a continuous-time signal observed in the interval  $(0, T]$ , modelled as a continuous process  $z(t)$  and perturbed by i.i.d. Gaussian noise  $\nu(t)$ ,

$$y(t) = z(t) + \nu(t). \quad (1)$$

Popular frameworks include modeling 1) the evolution of  $z(t)$  as a stochastic differential equation (SDE) or 2)  $z(t)$  as a GP realization. We focus on Eq. 1 sampled at  $\Delta$  intervals, i.e.,  $\mathbf{y}_k = y(k\Delta)$  and  $\mathbf{z}_k = z(k\Delta)$ ,

$$\mathbf{y}_k = \mathbf{z}_k + \nu_k. \quad (2)$$

This connection is important, as the parameters of Eq. 2, such as the transition and state covariance matrices associated with  $\mathbf{z}_k$ , are derived from Eq. 1. We use this link in the discussion of the properties of the PLSO model in Section 3.

### 2.3 Piecewise local stationarity

The concept of *piecewise local stationarity* (PLS) for nonstationary time-series with slowly time-varying spectra [Adak, 1998] plays an important role in the PLSO model. A stationary process has a constant mean and a covariance function which depends only on the difference between two time points.

The definition of PLS is involved, but it suffices to understand the following. It includes local stationary [Priestley, 1965, Dahlhaus, 1997] and amplitude-modulated stationary processes. More importantly, a PLS process can be approximated as a piecewise stationary (PS) process (Theorem 1 of [Adak, 1998])

$$z(t) = \sum_{m=1}^M \mathbf{1}(u_m \leq t < u_{m+1}) \cdot z^{(m)}(t), \quad (3)$$

where  $z^{(m)}(t)$  is a continuous stationary process and the breakpoints (boundaries) are  $0 = u_1 < \dots < u_{M+1} = T$ . By construction, Eq. 3 does not guarantee continuity across different PS intervals,

$$\lim_{t \rightarrow u_m^-} z(t) = \lim_{t \rightarrow u_m^-} z^{(m-1)}(t) \neq \lim_{t \rightarrow u_m^+} z^{(m)}(t) = \lim_{t \rightarrow u_m^+} z(t).$$

## 3 The PLSO generative model and its mathematical properties

Building on the Theorem 1 of [Adak, 1998], the PLSO framework models nonstationary data as PS processes. It is a superposition of  $J$  different PS processes  $\{\mathbf{z}_j\}_j$ , with  $\mathbf{z}_j$  corresponding to an oscillatory process centered at frequency  $\omega_j$ . PLSO also guarantees stochastic continuity across PS intervals. We show that piecewise stationarity and continuity across PS intervals are two competing objectives, and that PLSO strikes a balance between them, as discussed in Section 3.2.

Fig. 1 shows an example of the PLSO framework applied to simulated data. In the time domain, the inferred component using the regularized STFT (blue) [Kim et al., 2018], which imposes stochastic continuity on the STFT coefficients, suffers from discontinuity/distortion near window boundaries, whereas that inferred using the PLSO (red) does not. In the frequency domain, each PLSO component corresponds to a localized spectrum  $S_j(w)$ , the sum of which is the PSD  $\gamma(w)$ , which is fit to the data STFT  $I(w)$ . We start by introducing the PLSO model for a single window.

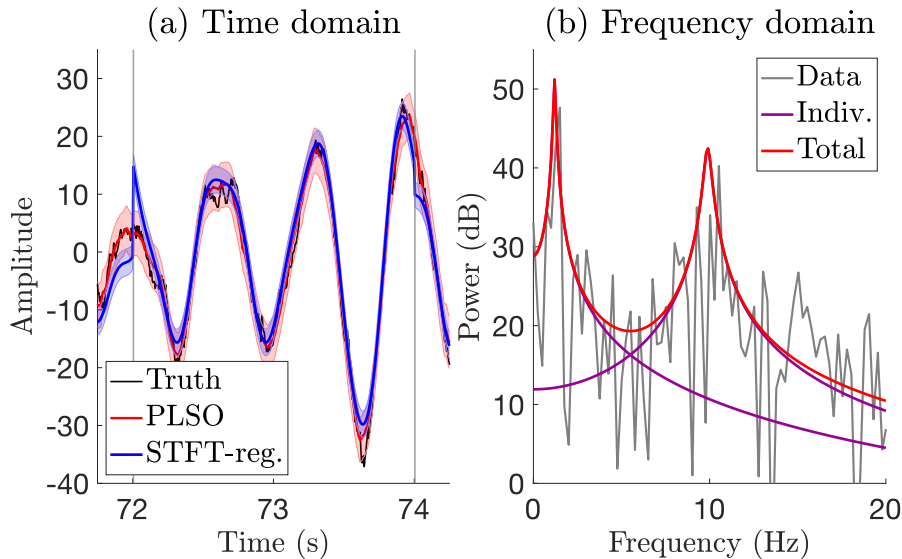


Figure 1: A simulated example. (a) Time domain. Data (black) around boundaries (gray) and inferred oscillatory component using PLSO (red) and regularized STFT (blue). (b) Frequency domain. Spectrum of the data (gray), PLSO-estimated components for  $J = 2$  (purple) and their sum (red).

### 3.1 PLSO for stationary data

As a building block for PLSO, we use the discrete stochastic harmonic oscillator model for a stationary time series [Qi et al., 2002, Cemgil and Godsill, 2005, Matsuda and Komaki, 2017]. The data  $\mathbf{y}$  are assumed to be a superposition of  $J$  zero-mean components

$$\begin{aligned} \mathbf{z}_{j,k}^{\text{vec}} &= \rho_j \mathbf{R}(\omega_j) \mathbf{z}_{j,k-1}^{\text{vec}} + \varepsilon_{j,k} \\ \mathbf{y}_k &= \mathbf{H} \mathbf{z}^k + \nu_k, \end{aligned} \quad (4)$$

where  $\mathbf{z}^k = (\mathbf{z}_{1,k}^{\Re} \quad \mathbf{z}_{1,k}^{\Im} \quad \cdots \quad \mathbf{z}_{J,k}^{\Re} \quad \mathbf{z}_{J,k}^{\Im})^T$ . We define the rotation matrix  $\mathbf{R}(\omega_j) = \begin{pmatrix} \cos(\omega_j) & -\sin(\omega_j) \\ \sin(\omega_j) & \cos(\omega_j) \end{pmatrix}$ , the gain  $\mathbf{H} = \begin{pmatrix} 1 & 0 & \cdots & 1 & 0 \end{pmatrix} \in \mathbb{R}^{2J}$ , the state noise  $\varepsilon_{j,k} \sim \mathcal{N}(0, \alpha_j \mathbf{I}_{2 \times 2})$ , and the observation noise  $\nu_k \sim \mathcal{N}(0, \sigma_\nu^2)$ .

We use  $\rho_j = \exp(-\Delta/l_j)$  and  $\alpha_j = \sigma_j^2(1 - \rho_j^2)$ . This establishes the equivalent continuous model in the form of SDE [Solin and Särkkä, 2014],

$$\frac{dz_j^{\text{vec}}(t)}{dt} = \underbrace{\left( \begin{pmatrix} -\frac{1}{l_j} \end{pmatrix} \oplus \begin{pmatrix} 0 & -\omega_j \\ \omega_j & 0 \end{pmatrix} \right)}_{\mathbf{F}} z_j^{\text{vec}}(t) + \varepsilon(t), \quad (5)$$

where  $z_j^{\text{vec}}(t) : \mathbb{R} \rightarrow \mathbb{R}^2$ ,  $\oplus$  denotes the Kronecker sum and  $\varepsilon(t) \sim \mathcal{N}(0, \sigma_j^2 \mathbf{I}_{2 \times 2})$ . Discretizing the solution of Eq. 5 at  $\Delta$ , such that  $\mathbf{z}_{j,k}^{\text{vec}} = z_j^{\text{vec}}(k\Delta)$ , yields Eq. 4. Consequently, we obtain the following for  $\Delta > 0$

$$\begin{aligned} \exp(\mathbf{F}\Delta) &= \exp(-\Delta/l_j) \mathbf{R}(\omega_j) \\ \sigma_j^2 \int_0^\Delta \exp(\mathbf{F}(\Delta - \tau)) \exp(\mathbf{F}(\Delta - \tau))^T d\tau &= \sigma_j^2 (1 - \exp(-2\Delta/l_j)) \mathbf{I}_{2 \times 2}. \end{aligned} \quad (6)$$

In the time domain, assuming the initial state covariance  $\mathbf{P}_j^1 = \sigma_j^2 \cdot \mathbf{I}_{2 \times 2} \quad \forall j$ , the autocovariance is given as  $\mathbb{E}[\mathbf{z}_{j,k}^{\Re} \mathbf{z}_{j,k+n'}^{\Re}] = \sum_{j=1}^J \sigma_j^2 \exp(-n' \Delta/l_j)$ . In the frequency domain, the spectra for the  $j^{\text{th}}$  component,  $S_j(\omega)$ , and the PSD for  $\mathbf{y}$ ,  $\gamma(\omega)$ , are given by

$$\begin{aligned} S_j(\omega) &= \phi_j(\omega) + \phi_j(-\omega), \quad \gamma(\omega) = \sigma_\nu^2 + \sum_{j=1}^J S_j(\omega) \\ \phi_j(\omega) &= \frac{\sigma_j^2 (1 - \exp(-2\Delta/l_j))}{1 + \exp(-2\Delta/l_j) - 2 \exp(-\Delta/l_j) \cos(\omega - \omega_j)}. \end{aligned}$$

The lengthscale  $l_j$  controls the bandwidth of the  $j^{\text{th}}$  process and  $\sigma_j^2$  controls the magnitude, along with  $l_j$ . The magnitude of  $S_j(\omega)$  is maximized at  $\omega = \pm \omega_j$ .

### 3.2 PLSO for nonstationary data

We first partition  $\mathbf{y}$  into  $M$  non-overlapping intervals of equal length  $N$ , such that  $K = MN$ . The PLSO generative model has three components

$$\begin{aligned} \log(\sigma_{j,m}^2) &= \log(\sigma_{j,m-1}^2) + (1/\lambda) \eta_{j,m} \quad (\text{Inter-window}) \\ \mathbf{z}_{j,mN+n}^{\text{vec}} &= \exp(-\Delta/l_j) \mathbf{R}(\omega_j) \mathbf{z}_{j,mN+(n-1)}^{\text{vec}} + \varepsilon_{j,mN+n} \quad (\text{Intra-window}) \\ \mathbf{y}_{mN+n} &= \mathbf{H} \mathbf{z}^{mN+n} + \nu_{mN+n} \quad (\text{Observation}), \end{aligned} \quad (7)$$

where  $\varepsilon_{j,mN+n} \sim \mathcal{N}(0, \sigma_{j,m}^2 (1 - \exp(-2\Delta/l_j)) \mathbf{I}_{2 \times 2})$ , with  $\nu_{mN+n}, \eta_{j,m} \sim \mathcal{N}(0, 1)$  and  $\mathbf{H}$  is as defined previously. We define  $\mathbf{P}_{j,m}^n$  as the covariance of  $\mathbf{z}_{j,mN+n}^{\text{vec}}$ . We additionally assume  $\mathbf{P}_{j,1}^1 = \sigma_{j,1}^2 \mathbf{I}_{2 \times 2}, \forall j$ .

The corresponding continuous model for  $\mathbf{z}_{j,mN+n}^{\text{vec}}$  is the same as Eq. 5, with different  $\mathbb{E}[\varepsilon_j(t)\varepsilon_j^T(t)] = \sum_{m=1}^M \sigma_{j,m}^2 \cdot \mathbf{1}\left(\left(\frac{m-1}{M}\right)T \leq t < \left(\frac{m}{M}\right)T\right) \mathbf{I}_{2 \times 2}$ .

The PLSO model exhibits Markovian dynamics on both the inter-window and intra-window levels. We assume constant lengthscale  $l_j$  to ensure that differences in the magnitude of  $S_j^{(m)}(\omega)$  across windows are caused only by differences in  $\{\sigma_{j,m}^2\}_{j,m}$ .

Given the generative model in Eq. 7, our goal is to perform inference on the posterior distribution

$$p\left(\{\mathbf{z}_j\}_j, \{\sigma_{j,m}^2\}_{j,m} \mid \mathbf{y}, \theta\right) = \underbrace{p\left(\{\sigma_{j,m}^2\}_{j,m} \mid \mathbf{y}, \theta\right)}_{\text{window-level posterior}} \cdot \underbrace{p\left(\{\mathbf{z}_j\}_j \mid \{\sigma_{j,m}^2\}_{j,m}, \mathbf{y}, \theta\right)}_{\text{sample-level posterior}}, \quad (8)$$

with the parameters  $\theta = \{\lambda, \sigma_\nu^2, \{l_j\}_j, \{\omega_j\}_j\}$ . We first analyze several properties of the PLSO model.

### 3.2.1 Stochastic continuity

We discuss two types of stochastic continuity, 1) at the window boundaries and 2) on  $\{\sigma_{j,m}^2\}$ .

**Continuity across the window boundaries** In the PLSO model, the state-space model for the entire time-series (Eq. 7) provides stochastic continuity across different PS intervals. The following proposition rigorously explains stochastic continuity for PLSO.

**Proposition 1.** *For a given  $m$ , as  $\Delta \rightarrow 0$ , the samples on either side of the interval boundary, which are  $\mathbf{z}_{(m+1)N}^{\text{vec}}$  and  $\mathbf{z}_{(m+1)N+1}^{\text{vec}}$ , become equivalent,*

$$\lim_{\Delta \rightarrow 0} \mathbf{z}_{(m+1)N}^{\text{vec}} = \lim_{\Delta \rightarrow 0} \mathbf{z}_{(m+1)N+1}^{\text{vec}}.$$

*Proof.* To analyze Eq. 7 in the limit of  $\Delta \rightarrow 0$ , we use the equivalent continuous model (Eq. 6). It suffices to show that  $\lim_{\Delta \rightarrow 0} \exp(\mathbf{F}\Delta) = \mathbf{I}_{2 \times 2}$  and  $\lim_{\Delta \rightarrow 0} \mathbb{E}[\varepsilon_{j,(m+1)N+1} \varepsilon_{j,(m+1)N+1}^T] = \mathbf{0}$ . We have,

$$\begin{aligned} \lim_{\Delta \rightarrow 0} \exp(\mathbf{F}\Delta) &= \mathbf{I}_{2 \times 2} + \lim_{\Delta \rightarrow 0} \sum_{k=1}^{\infty} \frac{\Delta^k}{k!} \mathbf{F}^k = \mathbf{I}_{2 \times 2} \\ \lim_{\Delta \rightarrow 0} \mathbb{E}[\varepsilon_{j,(m+1)N+1} \varepsilon_{j,(m+1)N+1}^T] / \sigma_{j,m+1}^2 &= \lim_{\Delta \rightarrow 0} \int_0^\Delta \exp(\mathbf{F}(\Delta - \tau)) \exp(\mathbf{F}(\Delta - \tau))^T d\tau = \mathbf{0}. \end{aligned}$$

□

This matches our intuition that as  $\Delta \rightarrow 0$ , the adjacent samples from the same process should get closer to each other until they become equivalent in the limit.

If  $\lim_{\Delta \rightarrow 0} \mathbf{z}_{(m+1)N}^{\text{vec}} \neq \lim_{\Delta \rightarrow 0} \mathbf{z}_{(m+1)N+1}^{\text{vec}}$ , the process is discontinuous, which is true for PS approaches without continuity. This remains true even when the parameters of different intervals are linked through deterministic or stochastic continuity constraints [Rosen et al., 2009, Ba et al., 2014, Kim et al., 2018, Song et al., 2018, Soulat et al., 2019] or using a hierarchical generative model [Gramacy and Lee, 2008].

We can interpret the continuity in the context of inference. For aforementioned PS approaches without continuity, the sample-level posterior factorizes as

$$\begin{aligned} p\left(\{\mathbf{z}_j\}_j \mid \mathbf{y}\right) &\propto p(\mathbf{y} \mid \{\mathbf{z}_j\}_j) \cdot p(\{\mathbf{z}_j\}_j) \\ &= \prod_{m=1}^M p\left(\mathbf{y}_{(m-1)N+1:mN} \mid \{\mathbf{z}_{j,(m-1)N+1:mN}\}_j\right) \cdot p\left(\{\mathbf{z}_{j,(m-1)N+1:mN}\}_j\right) \\ &\propto \prod_{m=1}^M p\left(\{\mathbf{z}_{j,(m-1)N+1:mN}\}_j \mid \mathbf{y}_{(m-1)N+1:mN}\right), \end{aligned} \quad (9)$$

where we dropped conditioning on  $\{\sigma_{j,m}^2\}_{j,m}$  and  $\theta$  for notational ease. Due to the absence of continuity,  $p(\{\mathbf{z}_j\}_j \mid \theta)$  factorizes as in the first equality. Consequently, the time-domain inference results are conditionally independent across the intervals. In PLSO, the time-domain estimates depend on the entire observation  $\mathbf{y}$ , not just on a subset, e.g.  $\mathbf{y}_{(m-1)N+1:mN}$ .

**Continuity on  $\sigma_{j,m}^2$**  For a given  $m$ , we impose stochastic continuity on  $\psi_{j,m} = \log(\sigma_{j,m}^2)$ . Effectively, this lets us pool together estimates of  $\{\sigma_{j,m}^2\}_m$  to 1) prevent overfitting to the noisy spectra and 2) estimate smooth dynamics of  $\{\sigma_{j,m}^2\}_m$ . The use of  $\log(\sigma_{j,m}^2)$ , rather than  $\sigma_{j,m}^2$ , ensures that  $\sigma_{j,m}^2$  is non-negative.

The choice of  $\lambda$  dictates the smoothness of  $\{\psi_{j,m}\}_m$ , with the two extremes corresponding to the familiar dynamics. If  $\lambda \rightarrow 0$ , we treat each window independently. If  $\lambda \rightarrow \infty$ , we treat the data as stationary, as the constraint forces  $\psi_{j,m} = \psi_j, \forall m$ .

### 3.2.2 Piecewise stationarity

For the  $m^{\text{th}}$  window to be piecewise stationary, the initial state covariance matrix  $\mathbf{P}_{j,m}^1$  should be the steady-state covariance matrix for the corresponding window,  $\mathbf{P}_{j,m}^1 = \mathbf{P}_{j,m}^\infty, \forall j, m$ . This ensures the covariance is stationary within each window.

The challenge is transitioning from  $\mathbf{P}_{j,m}^\infty$  to  $\mathbf{P}_{j,m+1}^\infty$ . If these were equal, a stationary model would apply to the data. Specifically, to ensure  $\mathbf{P}_{j,m+1}^1 = \mathbf{P}_{j,m+1}^\infty$ , given that  $\mathbf{P}_{j,m}^N = \mathbf{P}_{j,m}^\infty$ , the only solution is for the *variance* of the process noise between the two samples,  $\varepsilon_{j,(m+1)N+1}$ , to equal  $\mathbf{P}_{j,m+1}^\infty - \exp(-2\Delta/l_j) \mathbf{P}_{j,m}^\infty$ .

However, this is infeasible. First, if  $\mathbf{P}_{j,m+1}^\infty < \mathbf{P}_{j,m}^\infty$ , the variance is negative. Even if it were positive, the limit as  $\Delta \rightarrow 0$  does not equal zero, i.e.,  $\mathbf{P}_{j,m+1}^\infty - \mathbf{P}_{j,m}^\infty$ . Consequently, the Proposition 1 no longer holds and the trajectory is discontinuous. In summary, this implies that there exists a *trade-off* between maintaining piecewise stationarity and continuity across intervals.

PLSO maintains continuity across the intervals while ensuring that the state covariance quickly transitions to the steady-state covariance. We quantify the speed of transition in the following proposition.

**Proposition 2.** Assume  $l_j \ll N\Delta$ , such that  $\mathbf{P}_{j,m}^N = \mathbf{P}_{j,m}^\infty$ . In PLSO of Eq. 7, the difference between  $\mathbf{P}_{j,m}^\infty = \sigma_{j,m}^2 \mathbf{I}_{2 \times 2}$  and  $\mathbf{P}_{j,m+1}^\infty = \sigma_{j,m+1}^2 \mathbf{I}_{2 \times 2}$  decays exponentially fast as a function of  $n$ , for  $1 \leq n \leq N$ ,

$$\mathbf{P}_{j,m+1}^n = \mathbf{P}_{j,m+1}^\infty + \exp(-2n\Delta/l_j) (\mathbf{P}_{j,m}^\infty - \mathbf{P}_{j,m+1}^\infty).$$

*Proof.* We use a proof by induction. Details are in the **Appendix**. □

This implies that except for the transition portion at the beginning, we can assume stationarity for the rest of each window, with the autocovariance  $\mathbb{E} \left[ \mathbf{z}_{j,mN+n}^{\Re} \mathbf{z}_{j,mN+(n+n')}^{\Re} \right] = \sum_{j=1}^J \sigma_{j,m}^2 \exp(-n'\Delta/l_j)$  and PSD  $\gamma^{(m)}(\omega) = \sigma_{j,m}^2 + \sum_{j=1}^J S_j^{(m)}(\omega)$ . In practice, we can additionally impose a bound constraint on  $l_j$  during estimation and also use a reasonably-large  $N$ . We empirically observe that the existence of the transition period has little impact on the results.

## 4 Inference

The posterior distribution factorizes into two terms as mentioned in Eq. 8: The *window-level* posterior  $p(\{\sigma_{j,m}^2\}_{j,m} | \mathbf{y}, \theta)$  and the *sample-level* posterior  $p(\{\mathbf{z}_j\}_j | \{\sigma_{j,m}^2\}_{j,m}, \mathbf{y}, \theta)$ . This factorization suggests that we can break the inference into two stages.

**Stage 1** We minimize the *window-level* negative log-posterior, with respect to  $\theta$  and  $\{\sigma_{j,m}^2\}_{j,m}$ .

**Stage 2** Given the estimates from stage 1, we perform inference on the *sample-level* posterior. This could be as simple as obtaining the mean trajectory  $\hat{\mathbf{z}}_j = \mathbb{E}[\mathbf{z}_j | \{\sigma_{j,m}^2\}_{j,m}, \mathbf{y}, \theta]$  and its credible intervals, or any statistical quantity of interest.

We examine each stage in the following sections. We define  $\Psi = [\psi_{1,1}, \dots, \psi_{1,M}, \dots, \psi_{J,M}] \in \mathbb{R}^{JM}$  and use  $\psi_{j,m} = \log(\sigma_{j,m}^2)$  and  $\sigma_{j,m}^2$ , as well as  $\Psi$  and  $\{\sigma_{j,m}^2\}_{j,m}$ , interchangeably.

### 4.1 Optimization of $p(\{\sigma_{j,m}^2\}_{j,m} | \mathbf{y}, \theta)$

We can further factorize the window-level posterior distribution as  $p(\Psi | \mathbf{y}, \theta) \propto p(\mathbf{y} | \Psi, \theta) p(\Psi | \theta)$ . Since the posterior is intractable, we instead minimize the negative log-posterior,  $-\log p(\Psi | \mathbf{y}, \theta)$ . For the log-likelihood  $f(\Psi; \theta) = \log p(\mathbf{y} | \Psi, \theta)$ , we use the *Whittle likelihood* [Whittle, 1953], which is nonconvex, in the frequency domain,

$$f(\Psi; \theta) = -\frac{1}{2} \sum_{m=1}^M \sum_{n=1}^N \left\{ \log \gamma^{(m)}(\omega_n) + \frac{I^{(m)}(\omega_n)}{\gamma^{(m)}(\omega_n)} \right\}, \quad (10)$$

with discrete frequency  $\omega_n = 2\pi n/N$ , and periodogram for the  $m^{\text{th}}$  window  $I^{(m)}(\omega_n)$ ,

$$I^{(m)}(\omega_n) = \left| \sum_{n'=1}^N \exp\left(-\frac{2\pi i(n'-1)(n-1)}{N}\right) \mathbf{y}_{mN+n'} \right|^2.$$

The Whittle likelihood enables frequency-domain parameter estimation as a computationally more efficient alternative to the time domain estimation [Turner and Sahani, 2014]. The log-prior  $g(\Psi; \theta) = \log p(\Psi | \theta)$ , which arises from the continuity on  $\{\sigma_{j,m}^2\}_{j,m}$ , is given as

$$g(\Psi; \theta) = -\lambda \sum_{j=1}^J \sum_{m=1}^M (\psi_{j,m} - \psi_{j,m-1})^2. \quad (11)$$

This yields the following nonconvex problem, with nonconvex  $-f(\Psi; \theta)$  and convex  $-g(\Psi; \theta)$

$$\min_{\Psi, \theta} -\log p(\Psi | \mathbf{y}, \theta) = \min_{\Psi, \theta} -f(\Psi; \theta) - g(\Psi; \theta). \quad (12)$$

We optimize Eq. 12 by block coordinate descent [Wright, 2015] on  $\Psi$  and  $\{\sigma_{j,m}^2\}_{j,m}$ . For  $\sigma_{j,m}^2$ ,  $\{l_j\}_j$ , and  $\{\omega_j\}_j$ , we minimize  $-f(\Psi; \theta)$ , since  $-g(\Psi; \theta)$  does not affect these parameters. We perform conjugate gradient descent on  $\{l_j\}_j$  and  $\{\omega_j\}_j$ . Then, we fit  $\lambda$  through cross-validation by assessing the likelihood on a held-out dataset, with  $\hat{\Psi}$  and  $\hat{\theta}$  fitted on the training dataset. The initialization steps are discussed in the **Appendix**.

#### 4.1.1 Optimization of $\Psi$

We introduce an algorithm to compute a local optimal solution of  $\Psi$  for the nonconvex optimization problem in Eq. 12, by leveraging the regularized temporal structure of  $\Psi$ . It extends the inexact accelerated proximal gradient (APG) method [Li and Lin, 2015], by solving the proximal step with a Kalman filter/smoothener [Kalman, 1960]. To see this, we note that computing the proximal operator for  $-g(\Psi; \theta)$  is equivalent to MAP estimation for  $J$  independent 1-dimensional linear Gaussian state-space models

$$\Psi^{(l+1)} = \text{prox}_{-\alpha^{(l)}g}(\mathbf{v}^{(l)}) = \arg \min_{\Psi} \left( -g(\Psi) + \frac{1}{2\alpha^{(l)}} \|\Psi - \mathbf{v}^{(l)}\|^2 \right) = \arg \min_{\Psi} \sum_{j=1}^J q_j, \quad (13)$$

where the  $j^{\text{th}}$  component  $q_j$  is given as,

$$q_j = \sum_{m=1}^M \frac{(v_{j,m}^{(l)} - \psi_{j,m})^2}{2\alpha^{(l)}} + \lambda(\psi_{j,m} - \psi_{j,m-1})^2,$$

with  $v_{j,m}^{(l)} = \psi_{j,m}^{(l)} + \alpha^{(l)} (\partial f(\Psi; \theta) / \partial \psi_{j,m})|_{\Psi=\Psi^{(l)}}$ ,  $\mathbf{v}^{(l)} = [v_{1,1}^{(l)}, \dots, v_{1,M}^{(l)}, \dots, v_{J,1}^{(l)}, \dots, v_{J,M}^{(l)}] \in \mathbb{R}^{JM}$ , and  $\alpha^{(l)} > 0$  is a step-size for the  $l^{\text{th}}$  iteration.

The  $j^{\text{th}}$  optimization problem is equivalent to estimating the mean  $\{\psi_{j,m}\}_m$  of the posterior in a linear Gaussian state-space model with observations  $\{v_{j,m}^{(l)}\}_m$ , observation noise variance  $\alpha^{(l)}$ , and state variance  $1/2\lambda$ . Therefore, the solution can efficiently be computed with  $J$  parallel, 1-dimensional, Kalman filters/smoothers, with the computational complexity of  $O(JM)$ .

Note that Eq. 13 holds for all non-negative  $\lambda$ . If  $\lambda = 0$ , the proximal operator is an identity operator, as  $\psi_{j,m}^{(l+1)} = v_{j,m}^{(l)}$ . This is a gradient descent with step-size rule. If  $\lambda \rightarrow \infty$ , we have  $\psi_{j,m} = \psi_{j,m-1}$ ,  $\forall m$ , which leads to  $\psi_{j,m}^{(l+1)} = (1/M) \sum_{m=1}^M v_{j,m}^{(l)}$ . We can also replace  $g(\Psi; \theta)$  with more complicated priors, such as ones based on mixed norms [Kowalski, 2009, Ba et al., 2014] to promote group sparsity. This is possible since the algorithm iteratively approximates the complicated Whittle likelihood with a simpler/well-understood Gaussian likelihood, as in Eq. 13.

The algorithm is guaranteed to converge when  $\alpha^{(l)} < 1/C$ , where  $C$  is the Lipschitz constant for  $f(\Psi; \theta)$ . In practice, we select  $\alpha^{(l)}$  according to the step-size rule [Barzilai and Borwein, 1988]. In **Appendix**, we present the full algorithm for optimizing  $\Psi$  and a derivation for  $C$  under some assumptions.

## 4.2 Inference with $p(\{\mathbf{z}_j\}_j | \{\sigma_{j,m}^2\}_{j,m}, \mathbf{y}, \theta)$

Next, we perform inference on the sample-level posterior distribution  $p(\{\mathbf{z}_j\}_j | \hat{\Psi}, \mathbf{y}, \hat{\theta})$ . Since this is a Gaussian distribution, we can compute the mean trajectories  $\{\hat{\mathbf{z}}_j\}_j$  and the associated credible intervals analytically. Moreover, Eq. 7 is a linear Gaussian state-space model, we can use Kalman filter/smoothener for efficient computation. In **Appendix**, we discuss these steps.

We can also obtain posterior samples and perform Monte Carlo (MC) inference on any posterior-derived quantity. To generate the MC trajectory samples, we use the forward-filter backward-sampling (FFBS) algorithm [Carter and Kohn, 1994]. This is in contrast to generating samples from the interval-specific posterior in Eq. 9. In the latter case, the FFBS algorithm is run  $M$  separate times, the samples of which have to be pieced together to form an entire trajectory. With PLSO, the trajectory sample is conditioned on the entire observation and is continuous across the intervals.

One quantity of interest is the *phase*. We obtain the phase as  $\phi_{j,k} = \tan^{-1}(\mathbf{z}_{j,k}^{\Im} / \mathbf{z}_{j,k}^{\Re})$ . Since  $\tan^{-1}(\cdot)$  is a non-linear operation, we need to compute the mean trajectory and credible interval with MC samples, i.e., through the FFBS algorithm. Given the sample trajectories  $\{\mathbf{z}_j^{\text{vec},(s)}\}_{j,s}$  from the posterior, where  $s \in \{1, \dots, S\}$  denotes MC sample index, we estimate  $\hat{\phi}_{j,k} = (1/S) \sum_{s=1}^S \tan^{-1}(\hat{\mathbf{z}}_{j,k}^{\Im,(s)} / \hat{\mathbf{z}}_{j,k}^{\Re,(s)})$ , and use empirical quantiles for the associated credible interval.

## 5 Experiments

We apply PLSO to three settings: 1) A simulated dataset with slowly time-varying spectra, 2) local-field potential (LFP) data from the rat hippocampus, and 3) EEG data from a subject under anesthesia.

We use PLSO with  $\lambda = 0$ ,  $\lambda \rightarrow \infty$ , and  $\lambda$  determined by cross-validation,  $\lambda_{\text{CV}}$ . As baselines, we use

- **Regularized STFT (STFT-reg.)** This uses the STFT within a window, and a random-walk model to impose stochastic continuity of STFT coefficients across windows [Ba et al., 2014, Kim et al., 2018].

- **Piecewise stationary GP (GP-PS)** This computes GP kernels and time-domain estimates in a given window independently of others. For kernel parameters, we use the results from PLSO with  $\lambda = 0$ . Since  $\hat{\Psi}$  and  $\hat{\theta}$  are equivalent for PLSO and GP-PS, we can fully explain differences in time-domain estimates by the fact that the latter operate in the time-domain.

## 5.1 Simulated dataset

We simulate from the following model for  $1 \leq k \leq K$

$$\mathbf{y}_k = 10 \left( \frac{K-k}{K} \right) \mathbf{z}_{1,k}^{\Re} + 10 \cos^4(2\pi\omega_0 k) \mathbf{z}_{2,k}^{\Re} + \nu_k,$$

where  $\mathbf{z}_{1,k}$  and  $\mathbf{z}_{2,k}$  are as in Eq. 4, with  $\omega_0/\omega_1/\omega_2 = 0.04/1/10$  Hz,  $f_s = 200$  Hz,  $T = 100$  seconds,  $l_1 = l_2 = 1$ , and  $\nu_k \sim \mathcal{N}(0, 25)$ . This stationary process comprises two amplitude-modulated oscillations, namely one modulated by a slow-frequency sinusoid and the other a linearly-increasing signal [Ba et al., 2014]. Additional details are provided in the **Appendix**.

**Results** We simulate 20 realizations and train on each realization, assuming 2-second PS intervals. For PLSO, we use  $J = 2$ . The averaged results are shown in Table 1. We define  $\text{jump}(\mathbf{z}_j) = \frac{1}{M-1} \sum_{m=1}^{M-1} |\hat{\mathbf{z}}_{j,mN+1} - \hat{\mathbf{z}}_{j,mN}|$  to be the level of discontinuity at the interval boundaries. If  $\text{jump}(\mathbf{z}_j)$  greatly exceeds  $\text{jump}(\mathbf{z}_j^{\text{True}})$ , this implies the existence of large discontinuities at the boundaries.

For GP-PS and STFT-reg.,  $\text{jump}(\mathbf{z}_j)$  exceeds  $\text{jump}(\mathbf{z}_j^{\text{True}})$ , indicating discontinuities at the boundaries. An example is in Fig. 1. PLSO produces a similar jump metric as the ground truth metric, indicating the absence of discontinuities. We attribute the lower value to the Kalman smoothing operation.

Table 1: Simulation results. For  $\text{jump}(\mathbf{z}_j)$  and MSE, left/right metrics correspond to  $\mathbf{z}_1/\mathbf{z}_2$ , respectively.

	$\text{jump}(\mathbf{z}_j)$	MSE	IS div.
Truth	0.95/12.11	0/0	0
$\lambda = 0$	0.26/10.15	2.90/3.92	4.08
$\lambda \rightarrow \infty$	0.22/10.32	3.26/4.53	13.78
$\lambda = \lambda_{\text{CV}}$	0.25/10.21	<b>2.88/3.91</b>	<b>3.93</b>
STFT-reg.	49.59/81.00	6.89/10.68	N/A
GP-PS	16.99/23.28	3.00/4.04	4.08

For the TF domain, we use Itakura-Saito (IS) divergence [Itakura and Saito, 1970] as a distance measure between the ground truth spectra and the ones estimated using PLSO. That the highest divergence is given by  $\lambda \rightarrow \infty$  indicates the inaccuracy of the stationarity assumption. Furthermore,  $\lambda = \lambda_{\text{CV}}$  gives lower divergence than  $\lambda = 0$ , which indicates that the regularization helps estimate more accurate spectra.

## 5.2 LFP data from the rat hippocampus

We use LFP data collected from the rat hippocampus during open field tasks [Mizuseki et al., 2009], with  $T = 1,600$  seconds and  $f_s = 1,250$  Hz<sup>1</sup>. The theta neural oscillation band (5 ~ 10 Hz) is believed to play a role in coordinating the firing of neurons in the entorhinal-hippocampal system and is thus important for understanding the local circuit computation.

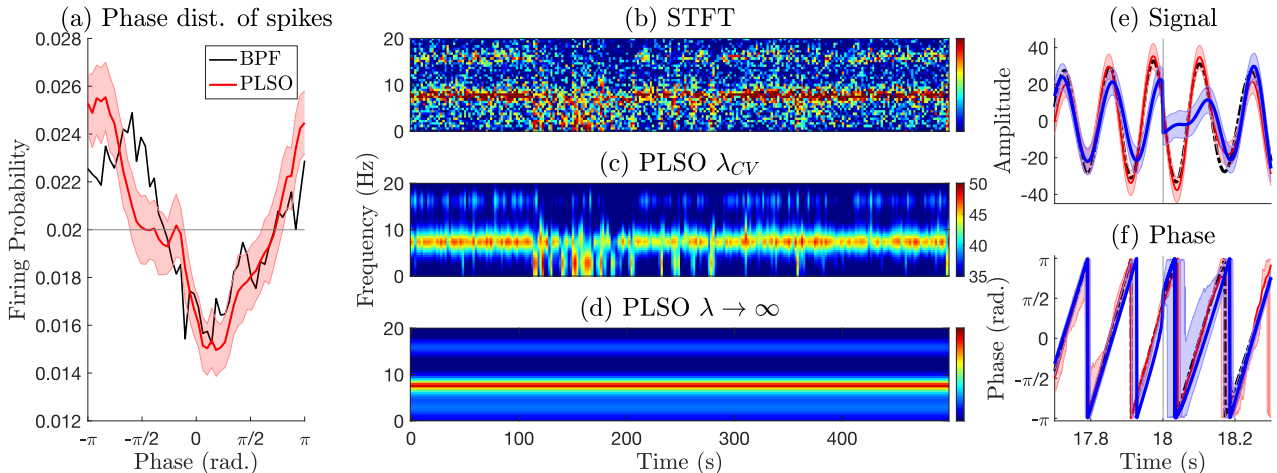


Figure 2: Result of analyses of hippocampal data. (a) Theta phase distribution of population neuron spikes, computed with bandpass-filtered LFP (black), PLSO estimate of  $\hat{\mathbf{z}}_2$  with credible interval estimated from 200 posterior samples (red). Horizontal gray line indicates uniform distribution. (b-d) Spectrogram (in dB) for 500 seconds with 2-second PS interval (b) STFT (c) PLSO with  $\lambda_{\text{CV}}$  (d) PLSO with  $\lambda \rightarrow \infty$ . Learned frequencies are  $\hat{\omega}_1/\hat{\omega}_2/\hat{\omega}_3 = 2.99/7.62/15.92$  Hz, with  $\hat{\omega}_4 \sim \hat{\omega}_6 > 25$  Hz. (e-f) Time-domain results. (e) Reconstructed signal (f) phase for  $\hat{\mathbf{z}}_2$  and interval boundary (vertical gray), with bandpass-filtered data (dotted black), STFT-reg. (blue), and PLSO (red). Shaded area represents 95% credible interval, computed from  $S = 200$  sample trajectories.

We fit PLSO with  $J = 6$ , assuming 2-second PS interval. The estimated  $\hat{\omega}_2$  is 7.62 Hz in the theta band. To obtain the phase for non-PLSO methods, we perform the Hilbert transform on the theta-band reconstructed signal. With no ground truth, we bandpass-filter (BPF) the data in the theta band for reference.

<sup>1</sup>We use channel 1 of mouse ec013.528 for the LFP data. The population spikes were simultaneously recorded from the same electrode.



**Spike-phase coupling** Fig. 2(a) shows the theta phase distribution of population neuron spikes in the hippocampus. The PLSO-estimated distribution (red) confirms the original study results analyzed with bandpass-filtering the signal (black) [Mizuseki et al., 2009] - the hippocampal spikes show a strong preference for a specific phase,  $\pi$  for this dataset, of the theta band. Since PLSO provides posterior sample-trajectories for the entire time-series, we can compute as many different realizations of the phase distribution as the number of MC samples. The resulting credible interval does not include the uniform distribution (horizontal gray), which suggests the statistical significance of strong phase preference.

**Denoised spectrogram** Fig. 2(b-d) shows the estimated spectrogram. We observe that PLSO denoises the spectrogram, while retaining sustained power at  $\hat{\omega}_2 = 7.62$  Hz and weaker bursts at  $\hat{\omega}_1/\hat{\omega}_3 = 2.99, 15.92$  Hz. However, the stationary PLSO ( $\lambda \rightarrow \infty$ ) is restrictive and fails to capture the change in the spectra around 100 ~ 200 seconds. PLSO with  $\lambda_{CV}$  captures the nonstationarity well.

**Time domain discontinuity** Fig. 2(e-f) show a segment of the estimated signal and phase near a boundary for  $\hat{\omega}_2$ . While the estimates from STFT-reg. (blue) and PLSO (red) follow the BPF result closely, the STFT-reg. estimates exhibit discontinuity/distortion near the boundary. In Fig. 2(f), the phase jump at the boundary is 38.4 degrees. Table 2 further corroborates this observation. We computed  $\text{jump}(\phi_2)$  for phase across all boundaries. Considering that the theta band roughly progress  $2.16 (= 7.5(\text{Hz}) \times 360/1250 (\text{Hz}))$  degrees per sample, we observe that BPF, as expected, and PLSO are not affected by the boundary effect. This is not the case for STFT-reg. and GP-PS.

Table 2:  $\text{jump}(\phi_2)$  (degrees/sample) for different approaches at boundaries for the hippocampus data.

$\lambda_{CV}$	$\lambda \rightarrow \infty$	STFT-reg.	GP-PS	BPF
2.40	2.66	26.83	25.91	2.23

### 5.3 EEG data from the human brain under propofol anesthesia

We apply our algorithm to the EEG data collected from a subject anesthetized with propofol anesthetic drug, to assess whether PLSO can leverage regularization to recover smooth spectral dynamics<sup>2</sup>. The EEG spectral dynamics are smooth throughout the induction of propofol anesthesia [Purdon et al., 2013]. The data last  $T = 2,300$  seconds, sampled at  $f_s = 250$  Hz. The drug infusion starts at  $t = 0$  second and the subject loses consciousness around  $t = 260$  second. We use  $J = 6$  and assume 4-second PS interval.

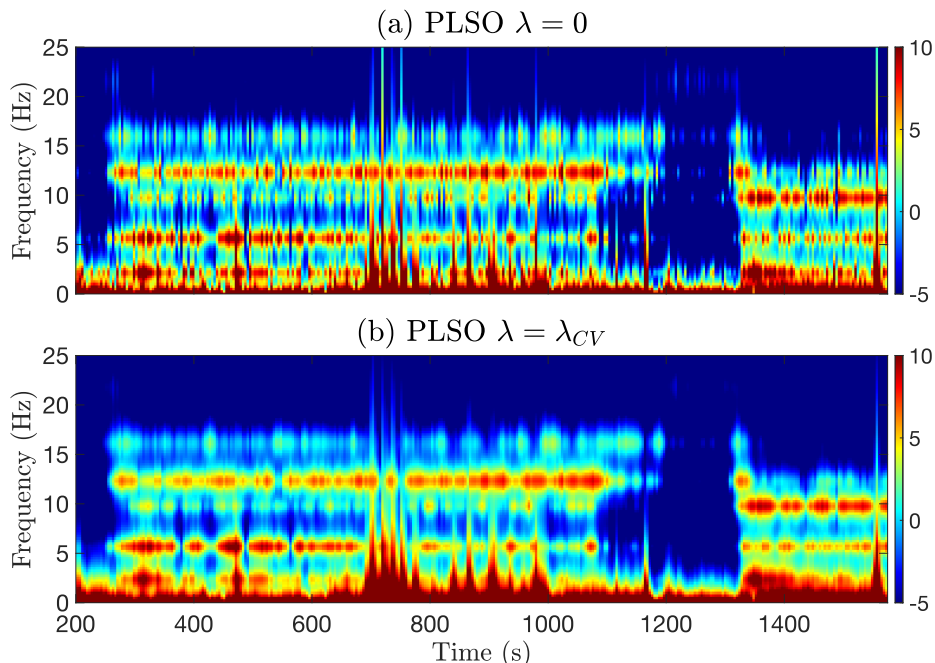


Figure 3: Spectrogram (in dB) under propofol anesthesia. (a) PLSO with  $\lambda = 0$  (b) PLSO with  $\lambda_{CV}$ .

**Smooth spectrogram** Fig. 3(a-b) shows a section of PLSO-estimated spectrogram with  $\lambda = 0$  and  $\lambda = \lambda_{CV}$ , respectively. They identify strong slow ( $0.1 \sim 2$  Hz) and alpha oscillations ( $8 \sim 15$  Hz), both well-known signatures of propofol-induced unconsciousness. We also observe that the alpha band power diminishes between 1,200 and 1,350 seconds, suggesting that the subject regained consciousness before becoming unconscious again. PLSO with  $\lambda = 0$  exhibits fluctuation in the power across time, since  $\{\sigma_{j,m}^2\}_{j,m}$  are fitted to each window independently. In contrast, PLSO with  $\lambda_{CV}$  exhibits smooth dynamics by pooling together PSD estimates from the neighboring windows. The regularization also helps remove movement-related artifacts, shown as vertical lines in Fig. 3(a), around 700 ~ 800/1,200 seconds, and spurious power in 20 ~ 25 Hz band. In summary, PLSO with regularization enables smooth spectral dynamics estimation and spurious noise removal.

<sup>2</sup>The EEG recording is part of de-identified data collected from patients at Massachusetts General Hospital (MGH) as a part of a MGH Human Research Committee-approved protocol.



## 6 Conclusion

We presented the Piecewise Locally Stationary Oscillatory (PLSO) framework to model nonstationary time-series data with slowly time-varying spectra, as the superposition of piecewise stationary (PS) oscillatory components. PLSO balances between stochastic continuity of the data across PS intervals and stationarity within each interval. For inference, we introduce an algorithm that combines Kalman theory and recent nonconvex optimization algorithms. Applications to simulated/real data show that PLSO preserves time-domain continuity and captures time-varying spectra. Future directions include 1) the automatic identification of PS intervals and 2) the expansion to higher-order autoregressive models and diverse priors on the parameters that enforce continuity across intervals.

## References

- [Adak, 1998] Adak, S. (1998). Time-dependent spectral analysis of nonstationary time series. *Journal of the American Statistical Association*, 93(444):1488–1501.
- [Ba et al., 2014] Ba, D., Babadi, B., Purdon, P. L., and Brown, E. N. (2014). Robust spectrotemporal decomposition by iteratively reweighted least squares. *Proceedings of the National Academy of Sciences*, 111(50):E5336–E5345.
- [Barzilai and Borwein, 1988] Barzilai, J. and Borwein, J. M. (1988). Two-Point Step Size Gradient Methods. *IMA Journal of Numerical Analysis*, 8(1):141–148.
- [Beck et al., 2018] Beck, A. M., Stephen, E. P., and Purdon, P. L. (2018). State space oscillator models for neural data analysis. In *2018 40th Annual International Conference of the IEEE Engineering in Medicine and Biology Society (EMBC)*, pages 4740–4743.
- [Carter and Kohn, 1994] Carter, C. K. and Kohn, R. (1994). On gibbs sampling for state space models. *Biometrika*, 81(3):541–553.
- [Cemgil and Godsill, 2005] Cemgil, A. T. and Godsill, S. J. (2005). Probabilistic phase vocoder and its application to interpolation of missing values in audio signals. In *2005 13th European Signal Processing Conference*, pages 1–4.
- [Dahlhaus, 1997] Dahlhaus, R. (1997). Fitting time series models to nonstationary processes. *Ann. Statist.*, 25(1):1–37.
- [Daubechies et al., 2011] Daubechies, I., Lu, J., and Wu, H.-T. (2011). Synchrosqueezed wavelet transforms: An empirical mode decomposition-like tool. *Applied and Computational Harmonic Analysis*, 30(2):243 – 261.
- [Gramacy and Lee, 2008] Gramacy, R. B. and Lee, H. K. H. (2008). Bayesian treed gaussian process models with an application to computer modeling. *Journal of the American Statistical Association*, 103(483):1119–1130.
- [Griffin and Jae Lim, 1984] Griffin, D. and Jae Lim (1984). Signal estimation from modified short-time fourier transform. *IEEE Transactions on Acoustics, Speech, and Signal Processing*, 32(2):236–243.
- [Huang et al., 1998] Huang, N. E., Shen, Z., Long, S. R., Wu, M. C., Shih, H. H., Zheng, Q., Yen, N.-C., Tung, C. C., and Liu, H. H. (1998). The empirical mode decomposition and the hilbert spectrum for nonlinear and non-stationary time series analysis. *Proceedings of the Royal Society of London. Series A: Mathematical, Physical and Engineering Sciences*, 454(1971):903–995.
- [Itakura and Saito, 1970] Itakura, F. and Saito, S. (1970). A statistical method for estimation of speech spectral density and formant frequencies.
- [Kalman, 1960] Kalman, R. (1960). A new approach to linear filtering and prediction problems. *Journal of Basic Engineering*.
- [Kim et al., 2018] Kim, S.-E., Behr, M. K., Ba, D., and Brown, E. N. (2018). State-space multitaper time-frequency analysis. *Proceedings of the National Academy of Sciences*, 115(1):E5–E14.
- [Kowalski, 2009] Kowalski, M. (2009). Sparse regression using mixed norms. *Applied and Computational Harmonic Analysis*, 27(3):303 – 324.
- [Le Roux et al., 2010] Le Roux, J., Vincent, E., Mizuno, Y., Kameoka, H., Ono, N., and Sagayama, S. (2010). Consistent wiener filtering: Generalized time-frequency masking respecting spectrogram consistency. In *Latent Variable Analysis and Signal Separation*, pages 89–96. Springer Berlin Heidelberg.
- [Li and Lin, 2015] Li, H. and Lin, Z. (2015). Accelerated proximal gradient methods for nonconvex programming. In *Advances in Neural Information Processing Systems 28*, pages 379–387. Curran Associates, Inc.
- [Lindsten and Schön, 2013] Lindsten, F. and Schön, T. B. (2013). *Backward Simulation Methods for Monte Carlo Statistical Inference*.
- [Matsuda and Komaki, 2017] Matsuda, T. and Komaki, F. (2017). Time series decomposition into oscillation components and phase estimation. *Neural Computation*, 29(2):332–367.
- [Mizuseki et al., 2009] Mizuseki, K., Sirota, A., Pastalkova, E., and Buzsaki, G. (2009). Theta oscillations provide temporal windows for local circuit computation in the entorhinal-hippocampal loop. *Neuron*, 64:267–280.
- [Oppenheim et al., 2009] Oppenheim, A. V., Schafer, R. W., and Buck, J. R. (2009). *Discrete-time Signal Processing (3rd Ed.)*. Prentice-Hall, Inc.
- [Priestley, 1965] Priestley, M. B. (1965). Evolutionary spectra and non-stationary processes. *Journal of the Royal Statistical Society. Series B (Methodological)*, 27(2):204–237.
- [Purdon et al., 2013] Purdon, P. L., Pierce, E. T., Mukamel, E. A., Prerau, M. J., Walsh, J. L., Wong, K. F. K., Salazar-Gomez, A. F., Harrell, P. G., Sampson, A. L., Cimenser, A., Ching, S., Kopell, N. J., Tavares-Stoeckel, C., Habeeb, K., Merhar, R., and Brown, E. N. (2013). Electroencephalogram signatures of loss and recovery of consciousness from propofol. 110(12):E1142–E1151.
- [Qi et al., 2002] Qi, Y., Minka, T. P., and Picard, R. W. (2002). Bayesian spectrum estimation of unevenly sampled nonstationary data. In *2002 IEEE International Conference on Acoustics, Speech, and Signal Processing*, volume 2, pages II–1473–II–1476.

- [Rasmussen and Williams, 2005] Rasmussen, C. E. and Williams, C. K. I. (2005). *Gaussian Processes for Machine Learning (Adaptive Computation and Machine Learning)*. The MIT Press.
- [Rosen et al., 2009] Rosen, O., Stoffer, D. S., and Wood, S. (2009). Local spectral analysis via a bayesian mixture of smoothing splines. *Journal of the American Statistical Association*, 104(485):249–262.
- [Solín and Särkkä, 2014] Solin, A. and Särkkä, S. (2014). Explicit Link Between Periodic Covariance Functions and State Space Models. In *Proceedings of the Seventeenth International Conference on Artificial Intelligence and Statistics*, volume 33 of *Proceedings of Machine Learning Research*, pages 904–912. PMLR.
- [Song et al., 2018] Song, A. H., Chakravarty, S., and Brown, E. N. (2018). A smoother state space multitaper spectrogram. In *2018 40th Annual International Conference of the IEEE Engineering in Medicine and Biology Society (EMBC)*, pages 33–36.
- [Soulat et al., 2019] Soulat, H., Stephen, E. P., Beck, A. M., and Purdon, P. L. (2019). State space methods for phase amplitude coupling analysis. *bioRxiv*.
- [Turner and Sahani, 2014] Turner, R. E. and Sahani, M. (2014). Time-frequency analysis as probabilistic inference. *IEEE Transactions on Signal Processing*, 62(23):6171–6183.
- [Whittle, 1953] Whittle, P. (1953). Estimation and information in stationary time series. *Ark. Mat.*, 2(5):423–434.
- [Wilkinson et al., 2019] Wilkinson, W. J., Riis Andersen, M., Reiss, J. D., Stowell, D., and Solin, A. (2019). Unifying probabilistic models for time-frequency analysis. In *ICASSP 2019 - 2019 IEEE International Conference on Acoustics, Speech and Signal Processing (ICASSP)*, pages 3352–3356.
- [Wilson and Adams, 2013] Wilson, A. G. and Adams, R. P. (2013). Gaussian process kernels for pattern discovery and extrapolation. In *Proceedings of the 30th International Conference on International Conference on Machine Learning - Volume 28, ICML’13*, page III–1067–III–1075.
- [Wilson et al., 2008] Wilson, K. W., Raj, B., Smaragdis, P., and Divakaran, A. (2008). Speech denoising using nonnegative matrix factorization with priors. In *2008 IEEE International Conference on Acoustics, Speech and Signal Processing*, pages 4029–4032.
- [Wright, 2015] Wright, S. J. (2015). Coordinate descent algorithms. *Mathematical Programming*, 151:3–34.

# Appendix for PLSO: A generative framework for decomposing nonstationary timeseries into piecewise stationary oscillatory components

References to the equations are made with respect to the equations in the supplementary materials. References to the sections in the section headings are made with respect to the sections in the main text.

## 7 Proof for Proposition 2 (Section 3.2.2)

**Proposition 2.** Assume  $l_j \ll N\Delta$ , such that  $\mathbf{P}_{j,m}^N = \mathbf{P}_{j,m}^\infty$ . In PLSO, the difference between  $\mathbf{P}_{j,m}^\infty = \sigma_{j,m}^2 \mathbf{I}_{2 \times 2}$  and  $\mathbf{P}_{j,m+1}^\infty = \sigma_{j,m+1}^2 \mathbf{I}_{2 \times 2}$  decays exponentially fast as a function of  $n$ , for  $1 \leq n \leq N$ ,

$$\mathbf{P}_{j,m+1}^n = \mathbf{P}_{j,m+1}^\infty + \exp(-2n\Delta/l_j) (\mathbf{P}_{j,m}^\infty - \mathbf{P}_{j,m+1}^\infty). \quad (14)$$

*Proof.* We first obtain the steady-state covariance  $\mathbf{P}_{j,m}^\infty$ . Since we assume  $\mathbf{P}_{j,1}^1 = \sigma_{j,1}^2 \mathbf{I}_{2 \times 2}$ , we can show that  $\forall m, n$ ,  $\mathbf{P}_{j,m}^n$  is a diagonal matrix, noting that  $\mathbf{R}(\omega_j) \mathbf{R}^T(\omega_j) = \mathbf{I}_{2 \times 2}$ . Denoting  $\mathbf{P}_{j,m}^\infty = \alpha \mathbf{I}_{2 \times 2}$ , we now use the discrete Lyapunov equation

$$\begin{aligned} \mathbf{P}_{j,m}^\infty &= \exp(-2\Delta/l_j) \mathbf{R}(\omega_j) \mathbf{P}_{j,m}^\infty \mathbf{R}^T(\omega_j) + \sigma_{j,m}^2 (1 - \exp(-2\Delta/l_j)) \mathbf{I}_{2 \times 2} \\ &\Rightarrow \alpha = \exp(-2\Delta/l_j) \alpha + \sigma_{j,m}^2 (1 - \exp(-2\Delta/l_j)) \\ &\Rightarrow \mathbf{P}_{j,m}^\infty = \sigma_{j,m}^2 \mathbf{I}_{2 \times 2}. \end{aligned} \quad (15)$$

We now prove the proposition by induction. For fixed  $j$  and  $m$ , and for  $n = 1$ ,

$$\begin{aligned} \mathbf{P}_{j,m+1}^1 &= \exp(-2\Delta/l_j) \mathbf{R}(\omega_j) \mathbf{P}_{j,m}^N \mathbf{R}^T(\omega_j) + \sigma_{j,m+1}^2 (1 - \exp(-2\Delta/l_j)) \mathbf{I}_{2 \times 2} \\ &= \{\sigma_{j,m+1}^2 + \exp(-2\Delta/l_j) (\sigma_{j,m}^2 - \sigma_{j,m+1}^2)\} \mathbf{I}_{2 \times 2}. \end{aligned}$$

Assuming the same holds for  $n = n' - 1$ , we have for  $n = n'$ ,

$$\begin{aligned} \mathbf{P}_{j,m+1}^{n'} &= \exp(-2\Delta/l_j) \mathbf{R}(\omega_j) \mathbf{P}_{j,m}^{(n'-1)} \mathbf{R}^T(\omega_j) + \sigma_{j,m+1}^2 (1 - \exp(-2\Delta/l_j)) \mathbf{I}_{2 \times 2} \\ &= \exp(-2\Delta/l_j) \sigma_{j,m+1}^2 \mathbf{I}_{2 \times 2} + \exp(-2n'\Delta/l_j) (\sigma_{j,m}^2 - \sigma_{j,m+1}^2) \mathbf{I}_{2 \times 2} + \sigma_{j,m+1}^2 (1 - \exp(-2\Delta/l_j)) \mathbf{I}_{2 \times 2} \\ &= \{\sigma_{j,m+1}^2 + \exp(-2n'\Delta/l_j) (\sigma_{j,m}^2 - \sigma_{j,m+1}^2)\} \mathbf{I}_{2 \times 2}. \end{aligned}$$

By the principle of induction, Eq. 14 holds for  $1 \leq n \leq N$ .  $\square$

## 8 Initialization for PLSO (Section 4)

We first construct a spectrogram of the data and empirically identify  $J$  and  $\{\omega_j^{\text{init}}\}_j$ . We observe that the result is robust to the choice of  $J$ , since redundant components converge to negligible magnitude. As for  $\{l_j^{\text{init}}\}_j$ , we set it to a certain fraction of corresponding  $\{\omega_j^{\text{init}}\}_j$ . We then fit  $\Psi$  and  $\theta$  with  $\lambda = 0$ . We finally use these estimates as initial values for other values of  $\lambda$ .

## 9 Optimization for $\Psi$ via proximal gradient update (Section 4.1.1)

We discuss the algorithm to obtain a local optimal solution  $\hat{\Psi}$  to the following nonconvex optimization problem

$$\begin{aligned} \min_{\Psi} \underbrace{-\log p(\Psi|\mathbf{y}, \theta)}_{h(\Psi; \theta)} &= \min_{\Psi} \underbrace{\frac{1}{2} \sum_{m=1}^M \sum_{n=1}^N \left\{ \log \gamma^{(m)}(\omega_n) + \frac{I^{(m)}(\omega_n)}{\gamma^{(m)}(\omega_n)} \right\}}_{-f(\Psi; \theta)} + \underbrace{\lambda \sum_{j=1}^J \sum_{m=1}^M (\psi_{j,m} - \psi_{j,m-1})^2}_{-g(\Psi; \theta)} \\ &= \min_{\Psi} -f(\Psi; \theta) - g(\Psi; \theta). \end{aligned} \quad (16)$$

The algorithm is described in Algorithm 1. It follows the steps outlined in the inexact accelerated proximal gradient algorithm [Li and Lin, 2015]. For faster convergence, we use larger step sizes with the Barzilai-Borwein (BB) step size initialization rule [Barzilai and Borwein, 1988]. For rest of this section, we drop dependence on  $\theta$ . The main novelty of our algorithm is the proximal gradient update

$$\begin{aligned} \mathbf{u}^{(l+1)} &= \text{prox}_{-\alpha_{\mathbf{w}}^{(l)} g} \left( \mathbf{w}^{(l)} + \alpha_{\mathbf{w}}^{(l)} \nabla f(\mathbf{w}^{(l)}) \right) = \arg \min_{\Psi} \left( \frac{1}{2\alpha_{\mathbf{w}}^{(l)}} \|\Psi - (\mathbf{w}^{(l)} + \alpha_{\mathbf{w}}^{(l)} \nabla f(\mathbf{w}^{(l)}))\|^2 - g(\Psi) \right) \\ &= \arg \min_{\Psi} \sum_{j=1}^J \left\{ \sum_{m=1}^M \left( \left( \mathbf{w}_{j,m}^{(l)} + \alpha_{\mathbf{w}}^{(l)} \cdot \frac{\partial f(\mathbf{w}^{(l)})}{\partial \mathbf{w}_{j,m}} \right) - \psi_{j,m} \right)^2 / (2\alpha_{\mathbf{w}}^{(l)}) + \lambda (\psi_{j,m} - \psi_{j,m-1})^2 \right\}, \end{aligned} \quad (17)$$

where the same holds for  $\mathbf{x}^{(l+1)} = \text{prox}_{-\alpha_{\Psi}^{(l)} g} \left( \Psi^{(l)} + \alpha_{\Psi}^{(l)} \nabla f(\Psi^{(l)}) \right)$ . The auxiliary variables  $\mathbf{w}, \mathbf{u}, \mathbf{x} \in \mathbb{R}^{JM}$  ensure convergence of  $\Psi$ . We use  $\mathbf{w}_{j,m}^{(l)}$  to denote  $((m-1)J + j)^{\text{th}}$  entry of  $\mathbf{w}^{(l)}$ . As mentioned in the main text, this can be solved in a computationally efficient manner by using Kalman filter/smoothing.

---

**Algorithm 1:** Inference for  $\Psi$  via inexact APG

---

**Result:**  $\hat{\Psi}$   
**Initialize**  $\Psi^{(0)} = \Psi^{(1)} = \mathbf{u}^{(1)}$ ,  $\beta^{(0)} = 0$ ,  $\beta^{(1)} = 1$ ,  $\delta > 0$ ,  $\rho < 1$   
**for**  $l \leftarrow 1$  **to**  $L$  **do**  
     $\mathbf{w}^{(l)} = \Psi^{(l)} + \frac{\beta^{(l-1)}}{\beta^{(l)}}(\mathbf{u}^{(l)} - \Psi^{(l)}) + \frac{\beta^{(l-1)} - 1}{\beta^{(l)}}(\Psi^{(l)} - \Psi^{(l-1)})$   
    **(BB step size initialization rule)**  
     $\mathbf{s}^{(l)} = \mathbf{u}^{(l)} - \mathbf{w}^{(l-1)}$ ,  $\mathbf{r}^{(l)} = -\nabla f(\mathbf{u}^{(l)}) + \nabla f(\mathbf{w}^{(l-1)})$   
     $\alpha_{\mathbf{w}}^{(l)} = \left( (\mathbf{s}^{(l)})^T \mathbf{s}^{(l)} \right) / \left( (\mathbf{s}^{(l)})^T \mathbf{r}^{(l)} \right)$   
     $\mathbf{s}^{(l)} = \mathbf{x}^{(l)} - \Psi^{(l-1)}$ ,  $\mathbf{r}^{(l)} = -\nabla f(\mathbf{x}^{(l)}) + \nabla f(\Psi^{(l-1)})$   
     $\alpha_{\Psi}^{(l)} = \left( (\mathbf{s}^{(l)})^T \mathbf{s}^{(l)} \right) / \left( (\mathbf{s}^{(l)})^T \mathbf{r}^{(l)} \right)$   
    **(Proximal update step)**  
    **repeat**  
    |  $\mathbf{u}^{(l+1)} = \text{prox}_{-\alpha_{\mathbf{w}}^{(l)} g} \left( \mathbf{w}^{(l)} + \alpha_{\mathbf{w}}^{(l)} \nabla f(\mathbf{w}^{(l)}) \right)$   
    |  $\alpha_{\mathbf{w}}^{(l)} = \rho \cdot \alpha_{\mathbf{w}}^{(l)}$   
    **until**  $h(\mathbf{u}^{(l+1)}) \leq h(\mathbf{w}^{(l)}) - \delta \|\mathbf{u}^{(l+1)} - \mathbf{w}^{(l)}\|^2$ ;  
    **repeat**  
    |  $\mathbf{x}^{(l+1)} = \text{prox}_{-\alpha_{\Psi}^{(l)} g} \left( \Psi^{(l)} + \alpha_{\Psi}^{(l)} \nabla f(\Psi^{(l)}) \right)$   
    |  $\alpha_{\Psi}^{(l)} = \rho \cdot \alpha_{\Psi}^{(l)}$   
    **until**  $h(\mathbf{x}^{(l+1)}) \leq h(\Psi^{(l)}) - \delta \|\mathbf{x}^{(l+1)} - \Psi^{(l)}\|^2$ ;  
     $\beta^{(l+1)} = \frac{1 + \sqrt{4(\beta^{(l)})^2 + 1}}{2}$   
     $\Psi^{(l+1)} = \begin{cases} \mathbf{u}^{(l+1)} & \text{if } h(\mathbf{u}^{(l+1)}) \leq h(\mathbf{x}^{(l+1)}) \\ \mathbf{x}^{(l+1)} & \text{otherwise} \end{cases}$   
**end**  
 $\hat{\Psi} = \Psi^{(L)}$

---

## 10 Lipschitz constant for $\nabla f(\Psi; \theta)$ (*Section 4.1.1*)

In this section, we prove that under some assumptions, we can show that the log-likelihood  $f(\Psi; \theta)$  has Lipschitz continuous gradient with the Lipschitz constant  $C$ . Let us start by restating the definition of Lipschitz continuous gradient.

**Definition 10.0.1.** A continuously differentiable function  $f : \mathcal{S} \rightarrow \mathbb{R}$  is Lipschitz continuous gradient if

$$\|\nabla f(\mathbf{x}) - \nabla f(\mathbf{y})\|_2 \leq C \|\mathbf{x} - \mathbf{y}\|_2 \quad \text{for every } \mathbf{x}, \mathbf{y} \in \mathcal{S}, \quad (18)$$

where  $\mathcal{S}$  is a compact subset of  $\mathbb{R}^{JM}$  and  $C > 0$  is the Lipschitz constant.

Our goal is to find the constant  $C$  for the Whittle likelihood  $f(\Psi; \theta)$

$$\begin{aligned}
 f(\Psi; \theta) &= -\frac{1}{2} \sum_{m=1}^M \sum_{n=1}^N \left\{ \log \gamma_{m,n} + \frac{I_{m,n}}{\gamma_{m,n}} \right\} \\
 &= -\frac{1}{2} \left\{ \underbrace{\sum_{m=1}^M \sum_{n=1}^N \log \left( \sigma_{\nu}^2 + \sum_{j=1}^J \exp(\psi_{j,m}) \alpha_{j,n} \right)}_{f_1(\Psi; \theta)} + \underbrace{\sum_{m=1}^M \sum_{n=1}^N \frac{I_{m,n}}{\left( \sigma_{\nu}^2 + \sum_{j=1}^J \exp(\psi_{j,m}) \alpha_{j,n} \right)}}_{f_2(\Psi; \theta)} \right\}, \quad (19)
 \end{aligned}$$

where we use  $I_{m,n} = I^{(m)}(\omega_n)$  for notational simplicity and

$$\alpha_{j,n} = \frac{(1 - \exp(-2\Delta/l_j))}{1 + \exp(-2\Delta/l_j) - 2 \exp(-\Delta/l_j) \cos(\omega_n - \omega_j)}.$$

We make the following assumptions

1.  $I_{m,n}$  is bounded, i.e.,  $I_{m,n} \leq C_I$ . With the real-world signal, we can reasonably assume that  $I_{m,n}$  or energy of the signal is bounded.
2.  $\forall j, m$ ,  $\psi_{j,m}$  is bounded, i.e.,  $|\psi_{j,m}| \leq \log C_{\psi}$  for some  $C_{\psi} > 1$ . This implies  $1/C_{\psi} \leq \exp(\psi_{j,m}) \leq C_{\psi}$ .

In addition, we have the following facts

1.  $I_{m,n}$ ,  $\alpha_{j,n}$ , and  $\gamma_{m,n}$  are nonnegative.
2.  $I_{m,n}$  and  $\gamma_{m,n}$  are bounded. This follows from the aforementioned assumptions.
3. For given  $\{l_j\}_j$ , we have bounded  $\alpha_{j,n}$ . To see this, note that the maximum of  $\alpha_{j,n}$  is achieved at  $\omega_n = \omega_j$ ,

$$\max \alpha_{j,n} = \frac{(1 - \exp(-2\Delta/l_j))}{1 + \exp(-2\Delta/l_j) - 2 \exp(-\Delta/l_j)} = \frac{(1 + \exp(-\Delta/l_j))(1 - \exp(-\Delta/l_j))}{(1 - \exp(-\Delta/l_j))^2} = \frac{(1 + \exp(-\Delta/l_j))}{(1 - \exp(-\Delta/l_j))}. \quad (20)$$

Therefore, denoting  $l_{\max} = \max_j \{l_j\}$ ,

$$\max \alpha_{j,n} \leq \frac{(1 + \exp(-\Delta/l_{\max}))}{(1 - \exp(-\Delta/l_{\max}))} = C_{\alpha}. \quad (21)$$

Finally, we define  $\mathcal{S} = [-\log C_\psi, \log C_\psi] \subset \mathbb{R}^{JM}$ .

We want to compute the Lipschitz constant for  $\nabla f_1(\Psi)$  and  $\nabla f_2(\Psi)$  for  $\Psi, \bar{\Psi} \in \mathcal{S}$ , i.e.,

$$\|\nabla f_1(\Psi) - \nabla f_1(\bar{\Psi})\|_2 \leq C_1 \|\Psi - \bar{\Psi}\|_2 \text{ and } \|\nabla f_2(\Psi) - \nabla f_2(\bar{\Psi})\|_2 \leq C_2 \|\Psi - \bar{\Psi}\|_2, \quad (22)$$

where we dropped dependence on  $\theta$  for notational simplicity. Consequently, the triangle inequality yields

$$\|\nabla f(\Psi) - \nabla f(\bar{\Psi})\|_2 \leq \|\nabla f_1(\Psi) - \nabla f_1(\bar{\Psi})\|_2 + \|\nabla f_2(\Psi) - \nabla f_2(\bar{\Psi})\|_2 \leq (C_1 + C_2) \|\Psi - \bar{\Psi}\|_2. \quad (23)$$

### 10.1 Lipschitz constant $C_1$ for $\nabla f_1(\Psi)$

Let us examine  $f_1(\Psi)$  first. The derivative with respect to  $\psi_{j,m}$  is given as

$$\frac{\partial f_1(\Psi)}{\partial \psi_{j,m}} = \sum_{n=1}^N \alpha_{j,n} \cdot \underbrace{\frac{\exp(\psi_{j,m})}{\sigma_\nu^2 + \sum_{j'=1}^J \exp(\psi_{j',m}) \alpha_{j',n}}}_{\tilde{f}(\psi_{j,m})} = \sum_{n=1}^N \alpha_{j,n} \tilde{f}(\psi_{j,m}). \quad (24)$$

We now have

$$\left| \frac{\partial f_1(\Psi)}{\partial \psi_{j,m}} - \frac{\partial f_1(\bar{\Psi})}{\partial \psi_{j,m}} \right| = \sum_{n=1}^N |\alpha_{j,n}| \cdot \left| \tilde{f}(\psi_{j,m}) - \tilde{f}(\bar{\psi}_{j,m}) \right|. \quad (25)$$

Without loss of generality, we assume  $\psi_{j,m} \geq \bar{\psi}_{j,m}$ . We now apply the mean value theorem (MVT) to  $\tilde{f}(\psi_{j,m})$

$$\tilde{f}(\psi_{j,m}) - \tilde{f}(\bar{\psi}_{j,m}) = \tilde{f}'(\psi'_{j,m})(\psi_{j,m} - \bar{\psi}_{j,m}), \quad \text{where } \psi'_{j,m} \in [\bar{\psi}_{j,m}, \psi_{j,m}]. \quad (26)$$

We can compute and bound  $\tilde{f}'(\psi'_{j,m}) = d\tilde{f}(\psi'_{j,m})/d\psi'_{j,m}$  as follows

$$\begin{aligned} \tilde{f}'(\psi'_{j,m}) &= \frac{\exp(\psi'_{j,m})}{\sigma_\nu^2 + \sum_{j'=1}^J \exp(\psi'_{j',m}) \alpha_{j',n}} - \frac{\alpha_{j,n} \exp^2(\psi'_{j,m})}{\left(\sigma_\nu^2 + \sum_{j'=1}^J \exp(\psi'_{j',m}) \alpha_{j',n}\right)^2} \\ &= \frac{\exp(\psi'_{j,m})}{\sigma_\nu^2 + \sum_{j'=1}^J \exp(\psi'_{j',m}) \alpha_{j',n}} \underbrace{\left(1 - \frac{\alpha_{j,n} \exp(\psi'_{j,m})}{\sigma_\nu^2 + \sum_{j'=1}^J \exp(\psi'_{j',m}) \alpha_{j',n}}\right)}_{\leq 1} \\ &\leq \frac{\exp(\psi'_{j,m})}{\sigma_\nu^2 + \sum_{j'=1}^J \exp(\psi'_{j',m}) \alpha_{j',n}} \\ &\leq \frac{C_\psi}{\sigma_\nu^2}. \end{aligned} \quad (27)$$

Combining Eq. 26 and 27, we have

$$\sum_{n=1}^N |\alpha_{j,n}| \cdot \left| \tilde{f}(\psi_{j,m}) - \tilde{f}(\bar{\psi}_{j,m}) \right| = \sum_{n=1}^N |\alpha_{j,n}| \cdot \left| \tilde{f}'(\psi'_{j,m})(\psi_{j,m} - \bar{\psi}_{j,m}) \right| \leq \frac{NC_\alpha C_\psi}{\sigma_\nu^2} |\psi_{j,m} - \bar{\psi}_{j,m}|. \quad (28)$$

We thus have,

$$\|\nabla f_1(\Psi) - \nabla f_1(\bar{\Psi})\|_2^2 = \sum_{j=1}^J \sum_{m=1}^M \left( \frac{\partial f_1(\Psi)}{\partial \psi_{j,m}} - \frac{\partial f_1(\bar{\Psi})}{\partial \psi_{j,m}} \right)^2 \leq \left( \frac{JMN C_\alpha C_\psi}{\sigma_\nu^2} \right)^2 \|\Psi - \bar{\Psi}\|_2^2. \quad (29)$$

### 10.2 Lipschitz constant $C_2$ for $\nabla f_2(\Psi)$

Computing  $C_2$  proceeds in a similar manner to computing  $C_1$ . The derivative with respect to  $\psi_{j,m}$  is given as

$$\frac{\partial f_2(\Psi)}{\partial \psi_{j,m}} = - \sum_{n=1}^N I_{m,n} \alpha_{j,n} \cdot \underbrace{\frac{\exp(\psi_{j,m})}{\left(\sigma_\nu^2 + \sum_{j'=1}^J \exp(\psi_{j',m}) \alpha_{j',n}\right)^2}}_{\tilde{f}(\psi_{j,m})}. \quad (30)$$

We now have

$$\left| \frac{\partial f_2(\Psi)}{\partial \psi_{j,m}} - \frac{\partial f_2(\bar{\Psi})}{\partial \psi_{j,m}} \right| = \sum_{n=1}^N |I_{m,n} \alpha_{j,n}| \cdot \left| -\tilde{f}(\psi_{j,m}) + \tilde{f}(\bar{\psi}_{j,m}) \right|. \quad (31)$$

Without loss of generality, assume  $\psi_{j,m} \geq \bar{\psi}_{j,m}$ . To apply MVT, we need to compute and bound  $\tilde{f}'(\psi'_{j,m})$

$$\begin{aligned} \tilde{f}'(\psi'_{j,m}) &= \frac{\exp(\psi'_{j,m})}{\left(\sigma_\nu^2 + \sum_{j'=1}^J \exp(\psi'_{j',m}) \alpha_{j',n}\right)^2} - \frac{2\alpha_{j,n} \exp^2(\psi'_{j,m})}{\left(\sigma_\nu^2 + \sum_{j'=1}^J \exp(\psi'_{j',m}) \alpha_{j',n}\right)^3} \\ &= \frac{\exp(\psi'_{j,m})}{\left(\sigma_\nu^2 + \sum_{j'=1}^J \exp(\psi'_{j',m}) \alpha_{j',n}\right)^2} \underbrace{\left(1 - \frac{2\alpha_{j,n} \exp(\psi'_{j,m})}{\sigma_\nu^2 + \sum_{j'=1}^J \exp(\psi'_{j',m}) \alpha_{j',n}}\right)}_{\leq 1} \\ &\leq \frac{\exp(\psi'_{j,m})}{\left(\sigma_\nu^2 + \sum_{j'=1}^J \exp(\psi'_{j',m}) \alpha_{j',n}\right)^2} \\ &\leq \frac{C_\psi}{\sigma_\nu^4}. \end{aligned} \quad (32)$$

Applying MVT,

$$\sum_{n=1}^N |I_{m,n} \alpha_{j,n}| \cdot \left| -\tilde{f}(\psi_{j,m}) + \tilde{f}(\bar{\psi}_{j,m}) \right| = \sum_{n=1}^N |I_{m,n} \alpha_{j,n}| \cdot \left| \tilde{f}'(\psi'_{j,m})(\psi_{j,m} - \bar{\psi}_{j,m}) \right| \leq \frac{NC_I C_\alpha C_\psi}{\sigma_\nu^4} |\psi_{j,m} - \bar{\psi}_{j,m}|. \quad (33)$$

We thus have,

$$\|\nabla f_2(\Psi) - \nabla f_2(\bar{\Psi})\|_2^2 = \sum_{j=1}^J \sum_{m=1}^M \left( \frac{\partial f_2(\Psi)}{\partial \psi_{j,m}} - \frac{\partial f_2(\bar{\Psi})}{\partial \psi_{j,m}} \right)^2 \leq \left( \frac{JMNC_\alpha C_\psi C_I}{\sigma_\nu^4} \right)^2 \|\Psi - \bar{\Psi}\|_2^2. \quad (34)$$

Collecting the Lipschitz constants  $C_1$  and  $C_2$ , we finally have

$$\|\nabla f(\Psi) - \nabla f(\bar{\Psi})\|_2 \leq \underbrace{\frac{JMNC_\alpha C_\psi}{\sigma_\nu^2} \left( 1 + \frac{C_I}{\sigma_\nu^2} \right)}_C \|\Psi - \bar{\Psi}\|_2. \quad (35)$$

## 11 Inference with $p\left(\{\mathbf{z}_j\}_j \mid \{\sigma_{j,m}^2\}_{j,m}, \mathbf{y}, \theta\right)$ (Section 4.2)

We present the details for performing inference with the *sample-level* posterior,  $p\left(\{\mathbf{z}_j\}_j \mid \{\sigma_{j,m}^2\}_{j,m}, \mathbf{y}, \theta\right)$ . First, we present the Kalman filter/smoothing algorithm to compute the mean posterior trajectory, as well as the accompanying credible interval. Next, we present the forward filtering backward sampling (FFBS) algorithm [Carter and Kohn, 1994, Lindsten and Schön, 2013] to generate Monte Carlo (MC) sample trajectories.

First, we define additional notations.

- $\mathbf{z}_{j,k|k'}^{\text{vec}} = \mathbb{E}\left[\mathbf{z}_{j,k}^{\text{vec}} \mid \mathbf{y}_{1:k'}, \{\sigma_{j,m}^2\}_{j,m}, \theta\right] \in \mathbb{R}^2$ : Posterior mean of  $\mathbf{z}_{j,k}^{\text{vec}}$ . We are primarily concerned with three types: 1)  $\mathbf{z}_{j,k|k-1}^{\text{vec}}$ , the one-step prediction estimate, 2)  $\mathbf{z}_{j,k|k}^{\text{vec}}$ , the Kalman filter estimate, and 3)  $\mathbf{z}_{j,k|MN}^{\text{vec}}$ , the Kalman smoother estimate.
- $\mathbf{z}_{k|k'}^{\text{vec}} = \left( \left( \mathbf{z}_{1,k|k'}^{\text{vec}} \right)^T, \dots, \left( \mathbf{z}_{J,k|k'}^{\text{vec}} \right)^T \right)^T \in \mathbb{R}^{2J}$ : A collection of  $\{\mathbf{z}_{j,k|k'}^{\text{vec}}\}_j$  in a single vector.
- $\mathbf{P}_{j,k|k'} = \mathbb{E}\left[\left(\mathbf{z}_{j,k}^{\text{vec}} - \mathbf{z}_{j,k|k'}^{\text{vec}}\right)\left(\mathbf{z}_{j,k}^{\text{vec}} - \mathbf{z}_{j,k|k'}^{\text{vec}}\right)^T \mid \mathbf{y}_{1:k'}, \{\sigma_{j,m}^2\}_{j,m}, \theta\right] \in \mathbb{R}^{2 \times 2}$ : Posterior covariance of  $\mathbf{z}_{j,k}^{\text{vec}}$ . Just as in  $\mathbf{z}_{j,k|k'}^{\text{vec}}$ , we are interested in three types, i.e.,  $\mathbf{P}_{j,k|k-1}$ ,  $\mathbf{P}_{j,k|k}$ , and  $\mathbf{P}_{j,k|MN}$ .
- $\mathbf{P}_{k|k'} = \text{blkdiag}(\mathbf{P}_{1,k|k'}, \dots, \mathbf{P}_{J,k|k'}) \in \mathbb{R}^{2J \times 2J}$ : A block diagonal matrix of  $J$  posterior covariance matrices.
- $\mathbf{A} = \text{blkdiag}(\exp(-\Delta/l_1) \mathbf{R}(\omega_1), \dots, \exp(-\Delta/l_J) \mathbf{R}(\omega_J)) \in \mathbb{R}^{2J \times 2J}$ : A block diagonal transition matrix.
- $\mathbf{H} = (1, 0, \dots, 1, 0)$ : As defined in the main text, the observation gain.

### 11.1 Kalman filter/smoothing

The Kalman filter equations are given as

$$\begin{aligned} \mathbf{z}_{j,mN+n|MN+(n-1)}^{\text{vec}} &= \exp(-\Delta/l_j) \mathbf{R}(\omega_j) \mathbf{z}_{j,mN+(n-1)|MN+(n-1)}^{\text{vec}} \\ \mathbf{P}_{j,mN+n|MN+(n-1)} &= \exp(-2\Delta/l_j) \mathbf{R}(\omega_j) \mathbf{P}_{j,mN+(n-1)|MN+(n-1)} \mathbf{R}^T(\omega_j) + \sigma_{j,m}^2 (1 - \exp(-2\Delta/l_j)) \\ \mathbf{K}_{mN+n} &= \mathbf{P}_{mN+n|MN+(n-1)} \mathbf{H}^T (\mathbf{H} \mathbf{P}_{mN+n|MN+(n-1)} \mathbf{H}^T + \sigma_\nu^2)^{-1} \in \mathbb{R}^{2J} \quad (\text{Kalman gain}) \\ \mathbf{z}_{mN+n|MN+n}^{\text{vec}} &= \mathbf{z}_{mN+n|MN+(n-1)}^{\text{vec}} + \mathbf{K}_{mN+n} (\mathbf{y}_{mN+n} - \mathbf{H} \mathbf{z}_{mN+n|MN+(n-1)}^{\text{vec}}) \\ \mathbf{P}_{mN+n|MN+n} &= (\mathbf{I}_{2J \times 2J} - \mathbf{K}_{mN+n} \mathbf{H}) \mathbf{P}_{mN+n|MN+(n-1)}. \end{aligned} \quad (36)$$

Subsequently, the Kalman smoother equations are given as

$$\begin{aligned} \mathbf{C}_{mN+n} &= \mathbf{P}_{mN+n|MN+n} \mathbf{A}^T \mathbf{P}_{mN+(n+1)|MN+n}^{-1} \in \mathbb{R}^{2J \times 2J} \\ \mathbf{z}_{mN+n|MN}^{\text{vec}} &= \mathbf{z}_{mN+n|MN+n}^{\text{vec}} + \mathbf{C}_{mN+n} (\mathbf{z}_{mN+(n+1)|MN}^{\text{vec}} - \mathbf{z}_{mN+(n+1)|MN+n}^{\text{vec}}) \\ \mathbf{P}_{mN+n|MN} &= \mathbf{P}_{mN+n|MN+n} + \mathbf{C}_{mN+n} (\mathbf{P}_{mN+(n+1)|MN} - \mathbf{P}_{mN+(n+1)|MN+n}) \mathbf{C}_{mN+n}^T. \end{aligned} \quad (37)$$

To obtain the mean reconstructed trajectory for the  $j^{\text{th}}$  oscillatory component,  $\{\hat{\mathbf{y}}_{j,k}\}_k$ , we take the real part of the  $j^{\text{th}}$  component of the smoothed mean,  $\hat{\mathbf{y}}_{j,k} = \mathbf{e}_{2j-1}^T \cdot \mathbf{z}_{k|MN}^{\text{vec}}$ , where  $\mathbf{e}_{2j-1} \in \mathbb{R}^{2J}$  is a unit vector with the only non-zero value, equal to 1, at the entry  $2j-1$ .

The 95% credible interval for  $\hat{\mathbf{y}}_{j,k}$ , denoted as  $\text{CI}_{j,k}^{\text{lower}}/\text{CI}_{j,k}^{\text{upper}}$  for the upper/lower end, respectively, is given as

$$\begin{aligned} \text{CI}_{j,k}^{\text{upper}} &= \mathbf{e}_{2j-1}^T \cdot \mathbf{z}_{k|MN}^{\text{vec}} + 1.96 \cdot \sqrt{\mathbf{e}_{2j-1}^T \mathbf{P}_{k|MN} \mathbf{e}_{2j-1}} \\ \text{CI}_{j,k}^{\text{lower}} &= \mathbf{e}_{2j-1}^T \cdot \mathbf{z}_{k|MN}^{\text{vec}} - 1.96 \cdot \sqrt{\mathbf{e}_{2j-1}^T \mathbf{P}_{k|MN} \mathbf{e}_{2j-1}}. \end{aligned} \quad (38)$$

### 11.2 FFBS algorithm

To generate the MC trajectory samples from the posterior distribution, we use the FFBS algorithm. The steps are summarized in Algorithm 2, which uses the Kalman estimates derived in the previous section. We denote  $s = 1, \dots, S$  as the MC sample index.



---

**Algorithm 2:** FFBS algorithm for  $p\left(\{\mathbf{z}_j\}_j \mid \{\sigma_{j,m}^2\}_{j,m}, \mathbf{y}, \theta\right)$

---

**Result:**  $\left\{\mathbf{z}_k^{\text{vec},(s)}\right\}_{k,s}^{MN,S}$

**for**  $s \leftarrow 1$  **to**  $S$  **do**

    Sample  $\mathbf{z}_{MN}^{\text{vec},(s)}$  from  $\mathcal{N}\left(\mathbf{z}_{MN|MN}^{\text{vec}}, \mathbf{P}_{MN|MN}\right)$ .

**for**  $k \leftarrow MN - 1$  **to**  $1$  **do**

        Sample  $\mathbf{z}_k^{\text{vec},(s)}$  from  $\mathcal{N}\left(\tilde{\mu}_k, \tilde{\mathbf{P}}_k\right)$ , where

$$\tilde{\mu}_k = \mathbf{z}_{k|k}^{\text{vec}} + \mathbf{P}_{k|k} \mathbf{A}^T \mathbf{P}_{k+1|k}^{-1} \left(\mathbf{z}_{k+1}^{\text{vec},(s)} - \mathbf{A} \mathbf{z}_{k|k}^{\text{vec}}\right)$$

$$\tilde{\mathbf{P}}_k = \mathbf{P}_{k|k} - \mathbf{P}_{k|k} \mathbf{A}^T \mathbf{P}_{k+1|k}^{-1} \mathbf{A} \mathbf{P}_{k|k}.$$

**end**

**end**

---

## 12 Simulation experiment (*Section 5.1*)

We simulate from the following model for  $1 \leq k \leq K$

$$\mathbf{y}_k = 10 \left( \frac{K-k}{K} \right) \mathbf{z}_{1,k}^{\Re} + 10 \cos^4(2\pi\omega_0 k) \mathbf{z}_{2,k}^{\Re} + \nu_k,$$

where  $\mathbf{z}_{1,k}$  and  $\mathbf{z}_{2,k}$  are from the PLSO stationary generative model, i.e.,  $\sigma_{j,m}^2 = \sigma_j^2$ . The parameters are  $\omega_0/\omega_1/\omega_2 = 0.04/1/10$  Hz,  $f_s = 200$  Hz,  $T = 100$  seconds,  $l_1 = l_2 = 1$ , and  $\nu_k \sim \mathcal{N}(0, 25)$ . This stationary process comprises two amplitude-modulated oscillations, namely one modulated by a slow-frequency ( $\omega_0 = 0.04$  Hz) sinusoid and the other a linearly-increasing signal [Ba et al., 2014]. We assume a 2-second PS interval. For PLSO models, we use  $J = 2$  components and 5 block coordinate descent iterations for optimizing  $\theta$  and  $\Psi$ .

Fig. 4 shows the true data in the time domain and spectrogram results. Fig. 4(c) shows that although the regularized STFT detects activities around 1 and 10 Hz, it fails to delineate the time-varying spectral pattern. Fig. 4(d) shows that PLSO with stationarity ( $\lambda \rightarrow \infty$ ) assumption is too restrictive. Fig. 4(e), (f) show that both PLSO with independent window assumption ( $\lambda = 0$ ) and PLSO with cross-validated  $\lambda$  ( $\lambda = \lambda_{CV}$ ) are able to capture the dynamic pattern, with the latter being more effective in recovering the smooth dynamics across different PS intervals.

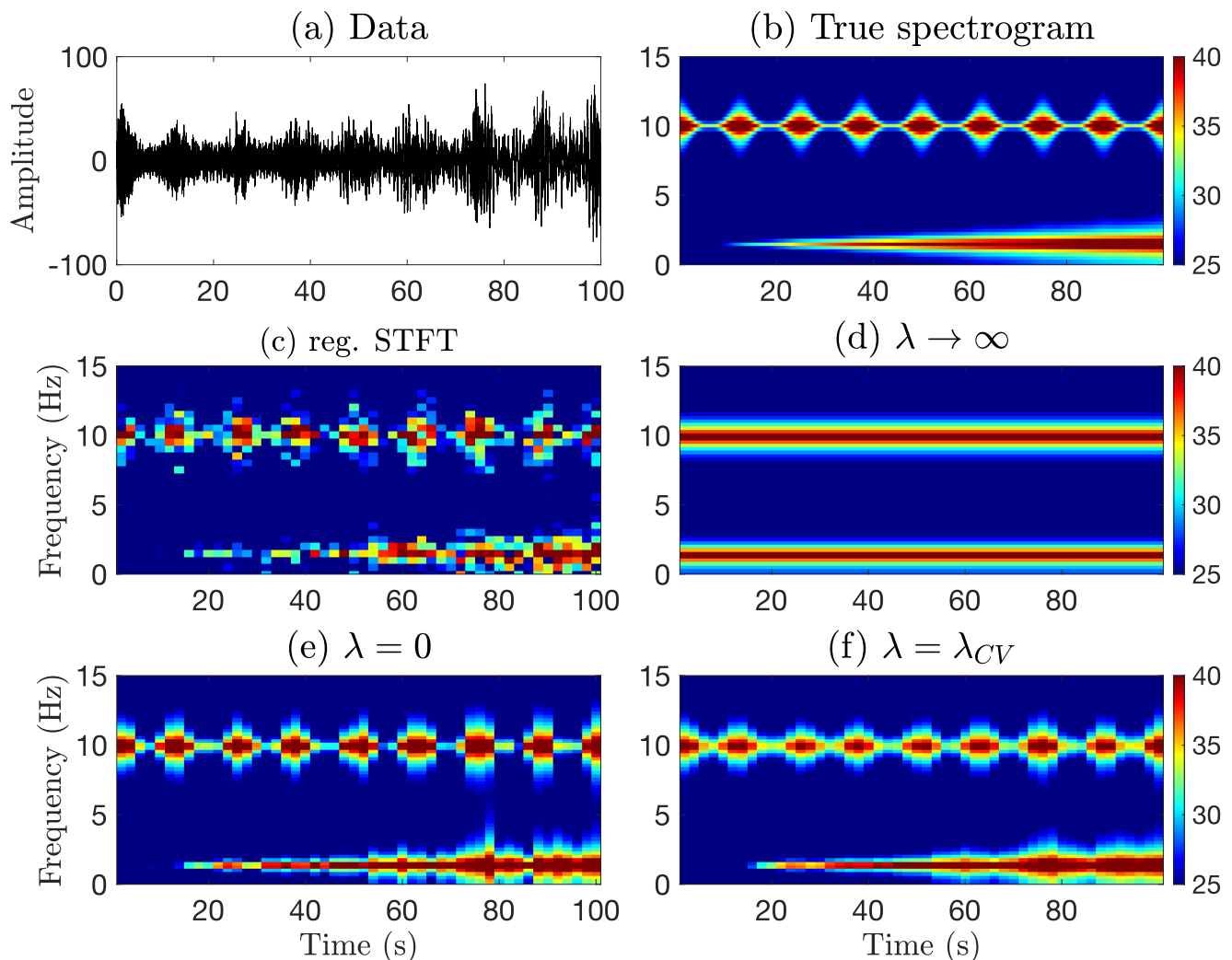


Figure 4: Simulation result with spectrograms (in dB). (a) True data (b) True spectrogram (c) regularized STFT (d) PLSO with  $\lambda \rightarrow \infty$  (e) PLSO with  $\lambda = 0$  (f) PLSO with  $\lambda = \lambda_{CV}$

### 13 Anesthesia EEG dataset (*Section 5.3*)

We show spectral analysis results for the EEG data of a subject anesthetized with propofol (This is a different subject from the main text.) The data last  $T = 2,500$  seconds, sampled at  $f_s = 250$  Hz. We assume a 4-second PS interval, use  $J = 9$  components and 5 block coordinate descent iterations for optimizing  $\theta$  and  $\Psi$ .

Fig. 5 shows the STFT and the PLSO-estimated spectrograms. As noted in the main text, PLSO with stationarity assumption is too restrictive and fails to capture the time-varying spectral pattern. Both PLSO with  $\lambda = 0$  and  $\lambda = \lambda_{CV}$  are more effective in capturing such patterns, with the latter able to remove the artifacts and better recover the smoother dynamics.

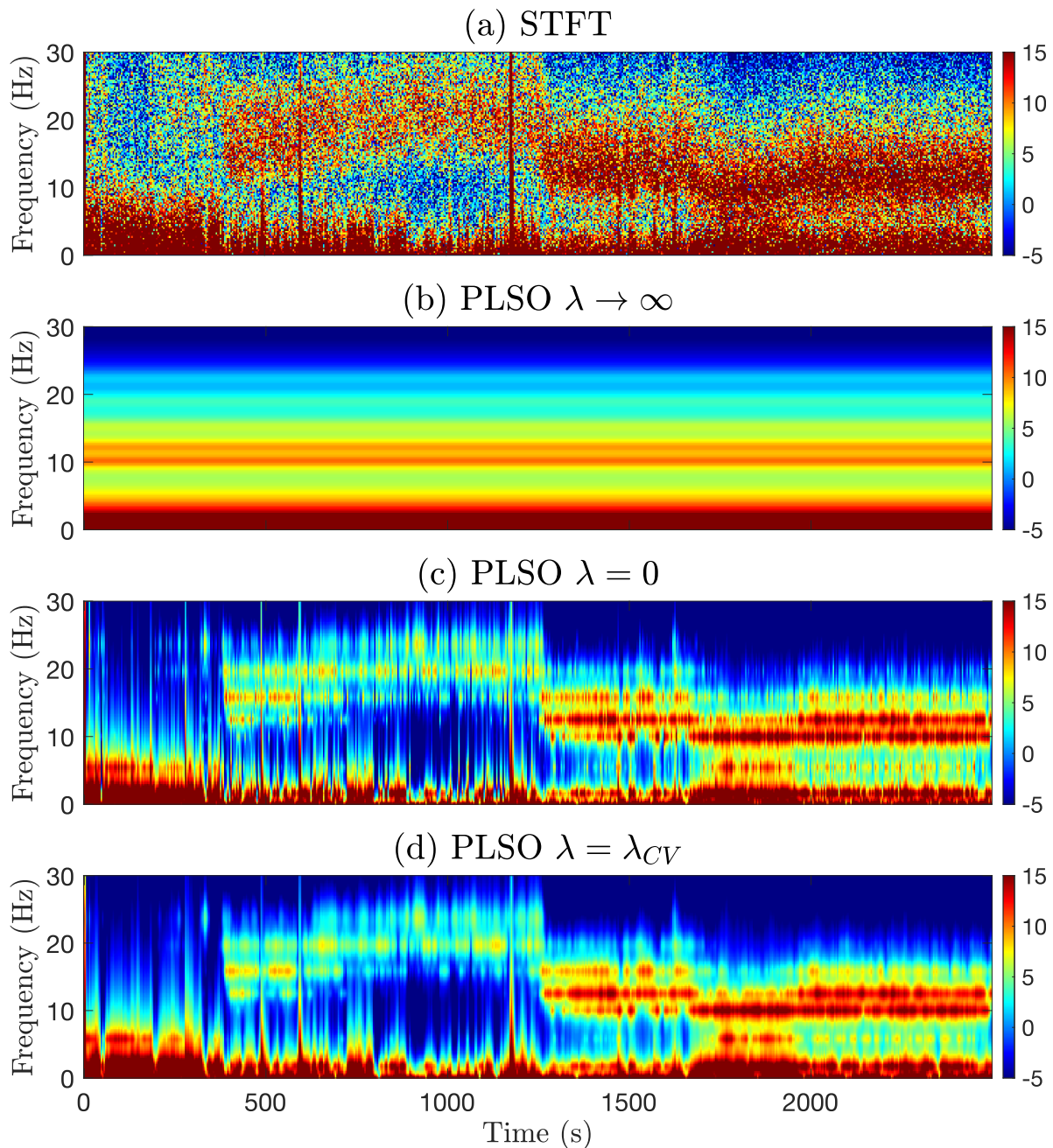


Figure 5: Spectrogram (in dB) under propofol anesthesia. (a) STFT of the data (b) PLSO with  $\lambda \rightarrow \infty$  (c) PLSO with  $\lambda = 0$  (d) PLSO with  $\lambda = \lambda_{CV}$ .